Mesopotamian Journal of Civil Engineering
Vol.2026, **pp**. 16–57
DOI: https://doi.org/10.58496/MJCE/2026/006; ISSN: 3006-1148
https://mesopotamian.press/journals/index.php/MJCE

Research Article

Assessment of the Impact of Oil-Contaminated Sand on the Structural Performance of Reinforced Concrete: Experimental and Numerical Analysis

Mustafa A. Saeed[1], Zarina Itam[2,3,*], Meqdam Hatem Hammadi Alakashe[1], Muhammad Imran Najeeb[4], Nazirul Mubin Zahari[2,3], Mohd Hafiz Zawawi[2,3], Nurul Husna Hassan[5]

[1] *College of Graduate Studies, Universiti Tenaga Nasional, Jalan IKRAM-UNITEN, Kajang 43000, Selangor, Malaysia.*
[2] *Department of Civil Engineering, College of Engineering, Universiti Tenaga Nasional, Jalan IKRAM-UNITEN, Selangor, Malaysia.*
[3] *Institute of Energy Infrastructure, Universiti Tenaga Nasional, Jalan IKRAM-UNITEN, 43000 Kajang, Selangor, Malaysia.*
[4] *Department of Engineering Education, Faculty of Engineering and Built Environment, Universiti Kebangsaan Malaysia, Selangor, Malaysia.*
[5] *Water Engineering and Management, Faculty of Civil and Environmental Engineering, Asian Institute of Technology (AIT), Thailand.*

ARTICLE INFO

Article History
Received 19 Jul 2026
Revised 15 Aug 2026
Accepted 04 Sep 2026
Published 27 Sep 2026

Keywords
Oil-contaminated sand concrete,
Crude oil,
RC beam,
Eco-friendly material,
Concrete Damaged Plasticity.

ABSTRACT

This study presents a systematic investigation of the physical, chemical, microstructural, and mechanical properties of oil-contaminated sand (OCS) and the resulting concrete, alongside a structural evaluation of RC beams under monotonic loading. Sixteen groups of concrete cylinders were cast at oil contamination levels of 0–30% by weight of fine aggregate, and six RC beams were fabricated and tested at contamination levels of 0%, 4%, 8%, 12%, 16%, and 20%. Physical testing showed OCS has an increase of 249% water absorption and a decrease in specific gravity of 7.3% compared to clean sand. At 2% oil content, there was a slight improvement in all mechanical properties of concrete, but as the content increased, the concrete properties gradually and nonlinearly decreased; at 30% oil content, the concrete compressive strength, splitting tensile strength, modulus of rupture and modulus of elasticity, were reduced by 70.91%, 89.94%, 71.43%, and 44.84%, respectively. From a structural point of view, a 70% decrease in cracking load, 61.1% decrease in ultimate load and 60% decrease in the deflection capacity at midspan were observed with contamination increasing from 0% to 20%, and a fundamental transition in failure mode from ductile flexural to explosive brittle failure. The practical limit for structural applications is determined as 8-12% contamination.

1. INTRODUCTION

As global demand for petroleum products has been rising, the search for crude oil, production, pipeline transmission, and refinery operations have continued to expand, resulting in an increasing number and size of crude oil spills on land. Near surface fine-grained sand in petroleum-producing countries such as Iraq, Arabian Gulf countries, Libya, Nigeria and Central Asia countries become contaminated by hydrocarbons annually via pipeline leaks, wellhead incidents, equipment failure and the migration of crude oil upward due to reservoir pressure [1], [2], [3] (see Fig. 1). After contamination, this sand is typically no longer suitable for use in conventional engineering applications because the hydrocarbons that adsorb to the grain surface change the geotechnical and physicochemical properties of the sand, which can lead to a reduction in shear strength and bearing capacity, an increase in compressibility and an excessive settlement and degradation of elements founded on or built with the sand [4]. A well-known environmental burden in petroleum-producing areas is the amount of crude oil-contaminated sand being produced on an annual basis, and the resources and technical know-how needed to clean up the contamination is always insufficient to meet the demand.

*Corresponding author. Email: iZarina@uniten.edu.my

(a) Sand field contaminated by oil

(b) Partial saturation of the sand

Fig. 1. Example of contaminated sand (Libya) [5]

The traditional remediation methods such as sand washing, bio-remediation, electrokinetic treatment, and thermal desorption are technically challenging, are time consuming, and often are not cost effective on the scale needed—often on the scale required by the problem [5]. These restrictions have encouraged increasing studies of alternative processes that channel contaminated sand to useful use in a building material instead of merely discarding it as a waste for disposal. Incorporation of oil-contaminated sand (OCS) into any cementitious system is a very attractive option both on environmental and resource conservation aspects as it will help to mitigate the environmental problem being faced and will conserve the scarce natural aggregates and can be economically beneficial to the extent site management expenses can be covered [6]. However, the approach is viable only if we really understand the engineering behaviour of the contaminated concrete, at both material and structural scales, and how it is affected by crude oil contamination, in a way that is rigorous and systematic.

The chemistry of the hydrocarbons that make up crude oil gives rise to complicated behaviour of the crude oil-contaminated sand. Crude oil is composed of a complex mixture of compounds, ranging from light volatile compounds to medium weight alkanes to heavy asphaltic residues with different proportions depending on the source geology, API gravity, and weathering after spillage. Crude oil molecules have the ability to attach to sand particle surfaces via van der Waals attraction and hydrogen bonding, creating a thin, but continuous film of crude oil molecules on the surface that alters the surface energy and engineering properties of the aggregate [7]. This coating increases apparent interparticle cohesion, at low contamination levels, typically less than 1–2% by weight, by partially filling pore space and by binding grains, similar to the apparent interparticle cohesion in the unsaturated fine-grained soils. Using direct shear tests, Abousnina et al. (2016) showed that the shear strength of fine sand is a local maximum at around 1% of light crude oil contamination where the apparent cohesion for the fine sand increases significantly [8], [9]. Al-Sanad and Ismael (2018) also discovered that the strength and stiffness of oil-sanded sand first increases with ageing, owing to the volatiles evaporating in the oil, leaving the remaining hydrocarbons to bind the grains more effectively [10]. However, at higher contamination levels, the cohesion enhancement is replaced by a progressive reduction of strength: the oil film thickens, interparticle friction gets less strong and the pore structure is filled up increasingly by hydrocarbons, which cannot be displaced mechanically or by capillarity [11]. Khamehchiyan et al. (2011) reported lower strength, permeability, dry density and Atterberg limits of both clayey and sandy soils under high contamination [12] and Khosravi et al. (2013) reported a reduction in frictional angle and compressibility at the same level of contamination [13]. This non-monotonic tendency, which translates as improvement with low contamination levels, progressive deterioration with high contamination levels, is also featured in literature from the geotechnical scale to the concrete material scale.

The interaction between the oil film and the cement hydration process determines the consequences of the incorporation of OCS in the concrete. The coating on contaminated aggregate surface is an impediment to the generation of calcium silicate hydrate (C–S–H) gel at the paste–aggregate interface and thereby reduces the strength of the interfacial transition zone (ITZ), which is the interphase between aggregate and Portland cement paste and is the weakest link in most hardened concrete. The results of Abdulhamid et al. [2] and Abousnina et al. (2018) [11] indicate that at 1% oil, the pore size and distribution decreased slightly from 454 µm average pore diameter in uncontaminated concrete to 368 µm in contaminated concrete, which corresponds to a densification of the microstructure as proposed by the cohesion-enhancement mechanism. However, as contamination increases from 2% to 20%, pore size increases progressively: to 446 µm at 2%, 500 µm at 6%, 720 µm at 10%, and 877 µm at 20% [11]. SEM micrographs show that at 10% contamination level, the ITZ between aggregates and the cement paste matrix is completely broken down to form a discrete micro-gap. Oil is hydrophobic, that is, the molecules prefer to be in contact with one another in preference to water, which results in a continuous layer of non-cohesion with water at the aggregate surface. The results of the XRD analyses of contaminated cement mortars confirm that the percentage of portlandite ($Ca(OH)_2$) increases with the increase in the amount of oil while the amount of C–S–H decreases, which is indicative of incomplete hydration; the percentage of silicon dioxide and calcium carbonate phase contents are also changed with the increase in the amount of oil due to the changes in the reactive environment [9], [14].

The workability of fresh concrete increases substantially with oil contamination. Slump values rise from 30 mm for uncontaminated concrete to 55, 95, 170, and 200 mm at contamination levels of 2.5%, 10%, 20%, and 25%, respectively [3]. This improvement, which reflects the lubricating action of oil on aggregate surfaces, is analogous to the effect of a chemical plasticiser. Osuji and Nwankwo [15] noted that the slump collapsed at 5% contamination, indicating collapse workability and potential segregation risk; they attributed the effect to crude oil interfering with cement–water binding reactions and delaying or preventing full cement hydration. While improved workability may appear beneficial in practice, it is accompanied by reduced mechanical performance in the hardened state and does not reflect any genuine improvement in the quality of the concrete matrix.

Much attention has been focused on the effect of OCS on the concrete compressive strength, but the results are not consistent in the published literature. The lack of consistency in reported results is due to variations in the types and API gravity of crude oil, sand mineralogy and permeability, contamination preparation procedure, curing regime, and specimen geometry, which makes it difficult to compare results between different studies. However, the overall trend is that, at very low contamination (around 0.5–1%), there is a marginal increase in compressive strength which is due to pore filling and optimum particle packing. Abousnina et al. [11] reported that there was a compressive strength gain of 3.2% when the light crude oil contamination level was 1%. For strengths above this optimum, the strength will drop off gradually and significantly. Reductions in 28-day compressive strength of 18–90% have been reported for contamination levels between 2.5% and 25%, with the rate of reduction accelerating at higher contamination levels. Osuji and Nwankwo [15] found that 1% crude oil contamination caused a 19.95% strength reduction in a 1:2:4 mix at 28 days, while Attom et al. [16] reported reductions of 32% and 42% for concrete with 1.5% kerosene- and diesel-contaminated fine aggregate, respectively. The governing mechanism is the progressive formation of oil films around both fine and coarse aggregate particles as contamination rises, reducing available bonding surface area between aggregates and cement paste, hindering hydration at the ITZ, and increasing entrapped void content as oil is displaced during curing.

Splitting tensile and flexural strengths follow similar trends but with higher sensitivity to oil contamination than compressive strength, a finding of considerable structural significance. Abousnina et al. [11] reported a 6.9% increase in splitting tensile strength at 1% oil content followed by reductions of 19%, 24%, 33%, and 70% at contamination levels of 2%, 6%, 10%, and 20%, respectively. The flexural strength for contaminated-site samples is also found to be progressive with values dropping from 5.87 N/mm² (control) to as low as 0.11 N/mm² at 25% contamination. This is because tensile and flexural failures are initiated at the tips of microcracks, which tend to be located at the weakest interfaces within the concrete matrix, while compressive failures occur throughout the mass of concrete due to the bulk resistance of the concrete mass and the fact that under compressive loading, the crack opening is balanced by the crack closure. The tensile-governed properties are more susceptible to contamination-induced interfacial weakening because the oil-degraded ITZ is the area where tensile cracks are expected to form. The modulus of elasticity is similarly affected: Diab [17], [18] showed that oil not only reduces compressive strength but also increases compressibility and decreases elastic stiffness, while Kadhum et al. [4] reported reductions in elastic modulus of 26.63% and 45.01% for normal-strength concrete immersed in kerosene and gas oil products, respectively.

Despite this accumulation of material-level evidence, the structural-level response of reinforced concrete members incorporating OCS has received remarkably little attention. The published literature on structural behaviour is limited to a small number of studies, none of which provides a wide-range or systematic investigation. Abousnina et al. [11] tested two

RC beams (1400 × 250 × 100 mm) at contamination levels of 0% and 6%, finding that the maximum load capacity of the contaminated beam was approximately 20% lower than the control, with earlier crack initiation and a shorter yielding period, while initial stiffness remained similar. Kadhum et al. [4] investigated the behaviour of reactive powder concrete and normal-strength concrete slabs soaked in kerosene and gas oil for 180 days, reporting that reactive powder concrete was largely unaffected (maximum load reduction of 2.58%) while normal concrete slabs lost 10–12.5% of ultimate load capacity after immersion. These studies are informative but limited in scope: they examine only one or two contamination levels, use immersion rather than aggregate-level contamination, and do not investigate the full range of structural performance metrics, stiffness, ductility, failure mode, energy absorption, steel–concrete bond behaviour, and load–strain response, that are necessary for structural design guidance. Crucially, none of these investigations spans a sufficiently wide contamination range to identify the threshold at which structural behaviour transitions from acceptable to unsafe.

This transition, from ductile flexural failure to brittle failure without warning, is the most consequential structural manifestation of oil contamination, and its threshold cannot be inferred from material testing alone. Structural codes have a requirement for ductility, as it gives occupants a visual and deformational warning to evacuate, and for emergency responders to respond, before collapse occurs. A loss of ductility in RC members containing OCS has not been quantified experimentally, and so has not been established what percentage of contamination is sufficient to cause this loss of ductility to be structurally critical. In addition, there is no published study that has conducted wide-range experimental characterisation and performed a nonlinear finite element modelling (FEM) along with a parametric study of structural design variables in the context of OCS concrete. For this reason, the present study was set to fill this gap altogether.

Specific objectives of this investigation are: (1) Characterising the physical, chemical, microstructural and mechanical properties of OCS and the resulting OCS concrete over the range of contamination levels (0-30% of FAC) (2) Evaluation of the load-deflection, load-strain, cracking pattern, failure mode and ductility of 6 RC beams with OCS at 0%, 4%, 8%, 12%, 16%, and 20% OCS by 0%–30% by weight of fine aggregate (3) Development, validation, and application of a nonlinear FEM using the Concrete Damaged Plasticity (CDP) framework in ABAQUS 2021 on the response of RC beams containing OCS over the range of contamination levels (0-30% of FAC) and a systematic parametric study, and (4) Identification of a contamination threshold value where the response of OCS concrete is structurally unsuitable, providing a quantitative evidence base for aggregate specification and sustainability policy in oil-affected areas.

This work has a novel aspect in three ways. It presents the first systematic dataset of the structural level for RC beams with OCS under 6 different contamination levels, covering the entire range of transition from ductile to brittle failure, and quantifying the reductions in load capacity, stiffness, ductility, and energy absorption. It introduces the first Concrete Damaged Plasticity finite element model that is calibrated for OCS concrete and validated with experimental tests on beams for all levels of contamination. It also sets out a clear contamination limit based on both material and structural evidence, furthering knowledge that is essential for regulatory guidance and material specification limits in petroleum contaminated areas.

2. RESEARCH SIGNIFICANCE

Across the petroleum-producing regions, vast amounts of fine-grained sand now have seismically altered chemical properties due to oil pollution, while clean sand for use in construction use is increasingly scarce. In these environments, the use of oil-contaminated sand is not a theoretical consideration but an economic and logistical reality and the lack of quantitative structural evidence to support its evaluation is a real safety void. That's why this study was conducted. It covers a broad spectrum of crude oil contamination and spans from the material scale up to the structural scale of full-scale reinforced concrete beams to provide the evidence base required by engineers, specifiers and regulators to make defensible decisions as to whether and within what limits, crude oil-contaminated sand can be accepted in construction practice.

The implications of this research are not limited to any single area but are applicable to multiple areas. With regard to resource and waste management, the study considers a hazardous material stream that has currently no cost-effective disposal pathway, and proposes contamination levels at which controlled reuse in non-structural and secondary construction applications may be technically possible. The establishment of an oil contamination level (8%, 12%) beyond which the ductile behaviour of the reinforced concrete beams is lost and transformed into brittle failure behavior has clear and compelling implications for buildings, infrastructure, and industrial structures in oil-contaminated regions in terms of structural safety. This ductility loss point can cause the concrete to fail without any warning which is not acceptable for the safety expectations that form the basis of current structural design codes. The validated nonlinear finite element model and the parametric study can be used to extrapolate to sets of beam configurations beyond those tested and provide a numerical tool capable of evaluating the performance of the structure for a variety of compressive strengths, reinforcement layouts, span lengths and boundary conditions that are common in the field. These papers collectively contribute to the development of the technical and regulatory knowledge base for the management of crude oil-contaminated aggregate as an engineering material, and for the exclusion of CCAA from structures where they can't be compromised for structural safety.

3. MATERIALS AND METHODS

The overall experimental and numerical programme is shown in Fig. 2, which aims to investigate the structural response of R.C using oil-contaminated sand (OCS) as fine aggregate substitution. Contaminated sand was prepared with crude oil from the Al-Kut refinery, Iraq, ranging from 0% to 30% by dry weight. The contaminated sand was then analysed for a full engineering characterisation programme including physical, chemical, environmental and microstructural testing, to determine its engineering properties and suitability and safety in a cementitious system. Concrete mixtures were then prepared at similar contamination levels, and fresh-state properties, such as workability, density, slump, and hardened-state properties such as compressive strength, splitting tensile strength, modulus of rupture, and modulus of elasticity were measured on standard specimens including cylinders, prisms, and cubes. The structural performance was assessed by conducting four-point bending tests on RC beam specimens fabricated in accordance with ACI 318M-19 and obtaining the load-deflection and load-strain data and failure modes for the entire range of contamination levels. The materials used were all local: cement, aggregate and steel reinforcement, and were all checked and verified against the relevant Iraqi Quality Standards (IQS No. 5/2019 and IQS No. 45/2019) before use.

A nonlinear finite element study was performed in ABAQUS 2021 whereafter the experimental investigation was completed. A 3D model, incorporating the Concrete Damaged Plasticity (CDP) constitutive model, was developed, calibrated and then applied in a parametric analysis to extend the results of the experimental tests beyond the tested configurations. The two programmes combine to provide an integrated methodology that can provide both quantitative performance data and mechanistic understanding of contaminated-sand concrete under realistic structural loading conditions.

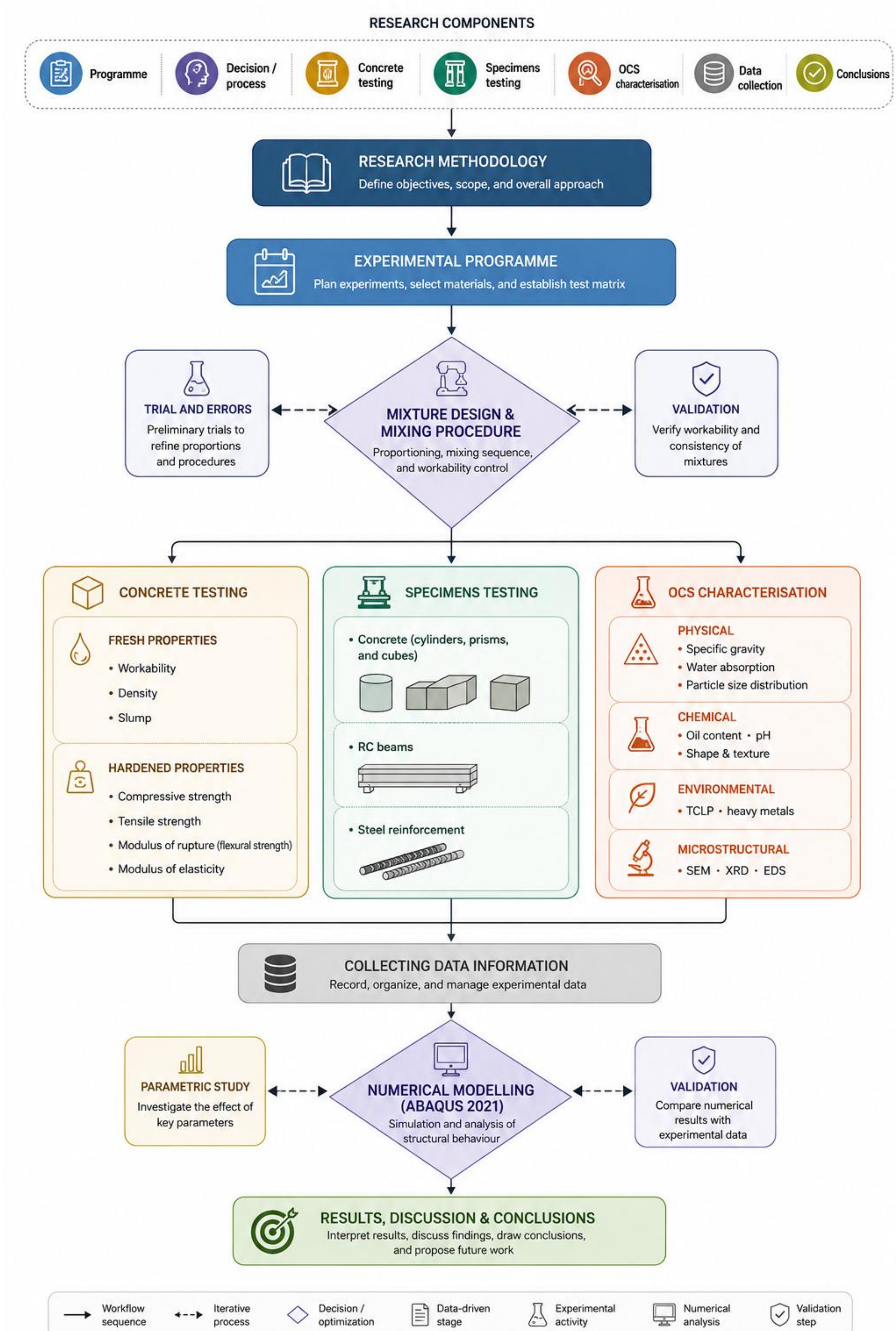

Fig. 2. Adopted program for the present research

3.1 Materials

3.1.1 Reinforced Concrete Materials

The cement used for all concrete mixes was Ordinary Portland Cement (OPC) type I (Table 1), whose chemical and physical properties were checked against the Iraqi Specification No. 5/2019; the cement had an initial setting time of 1.06 hours, a final setting time of 4.00 hours, a Lechatelier expansion of 0.7 mm, compressive strength of 27 MPa at 3 days old and 33 MPa at 7 days old, all within the permissible limits of the Iraqi cement specification and verified by the National Centre for Construction Laboratories and Researches. The fine aggregate was natural river sand with a maximum particle size of 4.75 mm, classified as Zone 2 under Iraqi Specification No. 45/2019, with a grading distribution of 94.82%, 80.12%, 58.00%, 45.44%, and 16.21% passing the 4.75, 2.36, 1.18, 0.60, and 0.30 mm sieves respectively, and a fines content of 3.14% passing the 75 µm sieve, below the 5% threshold prescribed by the standard (Table 2 and Fig. 3). Ordinary tap water is used to cast all specimens in the mixing and curing of concrete without any additives. The water used is pure and free of harmful substances such as oils, acids, alkalis, salts, and organic compounds. Longitudinal and transverse reinforcement in all beam specimens consisted of deformed steel bars with a nominal yield strength of 410 MPa and an elastic modulus of 200 GPa (Table 3).

TABLE I. CHEMICAL COMPOSITION AND PHYSICAL PROPERTIES OF CEMENT (OPC TYPE I, AL-MASS COMPANY, IRAQ)

Category	Property	Value	IQS No. 5/2019 Limit
Chemical composition	SiO_2	20.70%	—
	CaO	54.12%	—
	Al_2O_3	4.21%	—
	Fe_2O_3	3.65%	—
	MgO	4.00%	≤ 5.0%
	SO_3	2.07%	≤ 2.5%
	Loss on ignition (L.O.I)	3.00%	≤ 4.0%
	Insoluble residue (I.R.)	1.11%	≤ 1.5%
	Lime saturation ratio (L.S.R)	1.00	0.66–1.02
Physical properties	Initial setting time	1.06 h	≥ 45 min
	Final setting time	4.00 h	≤ 10 h
	Soundness, Lechatelier expansion	0.7 mm	≤ 0.8 mm
	Compressive strength, 3 days	27 MPa	≥ 15 MPa
	Compressive strength, 7 days	33 MPa	≥ 23 MPa
All values comply with the requirements of IQS No. 5/2019			

TABLE II. GRADING AND DELETERIOUS MATERIAL LIMITS FOR FINE AND COARSE AGGREGATES (IQS NO. 45/2019)

Sieve size (mm)	Fine aggregate, % passing	IQS limit (Zone 2)	Coarse aggregate, % passing	IQS limit (5–20 mm)
37.5	—	—	—	100
20	—	—	97.00	95–100
10	100	100	38.21	30–60
5	—	—	0.68	0–10
4.75	94.82	90–100	—	—
2.36	80.12	75–100	—	—
1.18	58.00	55–90	—	—
0.60	45.44	35–59	—	—
0.30	16.21	8–30	—	—
0.15	8.00	0–10	—	—
Material finer than 75 µm (%)	3.14	≤ 5.0	0.20	≤ 3.0
Sulphate content, SO_3 (%)	0.20	≤ 0.5	0.068	≤ 0.1
All values comply with the requirements of IQS No. 45/2019.				

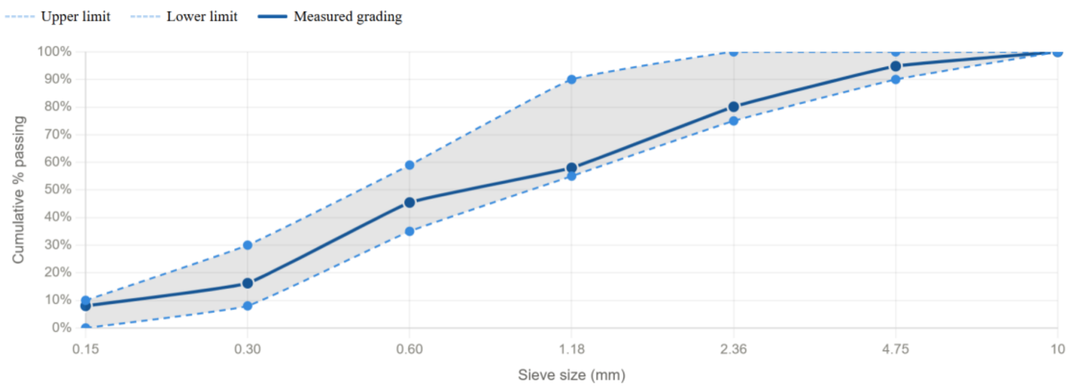

(a) Fine aggregate, Zone 2 (IQS No. 45/2019)

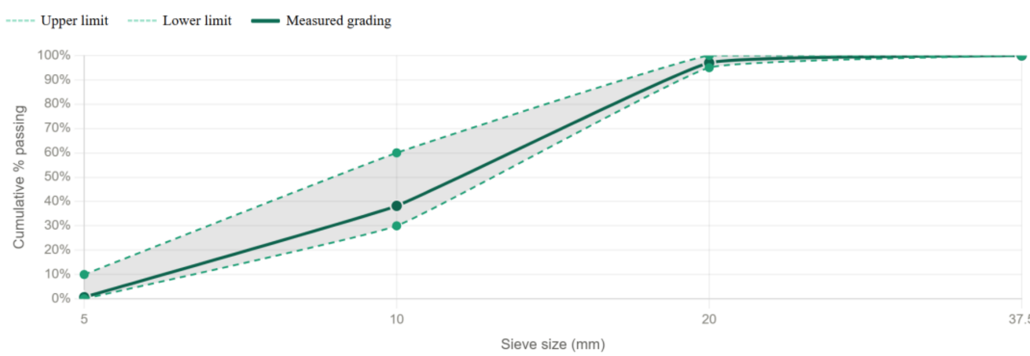

(b) Coarse aggregate, 5–20 mm (IQS No. 45/2019)

Fig. 3. Grading curves for fine and coarse aggregates compared against IQS No. 45/2019 limits. Both measured samples fall within the specified upper and lower grading envelopes.

TABLE III. PROPERTIES OF STEEL REINFORCEMENT.

D (mm)		Strength * (MPa)		Elongation(%)	Strain (%)		Es (GPa)	Density (kg/m³)	Mass (kg)	Area (mm²/m)
Nominal	Actual	Yield	Actual		Yield	Ultimate				
10	10.11	422.15	621.57	19.58	0.211	0.402	201,111	7855	0.63	80.3
* ASTM A615 Grade 60 ($f_y \geq$ 420 MPa (60.9 ksi))										

3.1.2 Physical Properties

3.1.2.1 Specific Gravity (SG) and Water Absorption (WA)

The physical properties of oil-contaminated sand (OCS) differ measurably from those of clean sand across all parameters examined, as summarised in Table 4. The increase in water absorption from 8.15% in clean sand to 28.43% in OCS was thought to be caused by the oil coating on the grain surface that modifies the interfacial energy and thereby increases water retention. The bulk density increased from 0.65 to 0.706 g/ml, which is attributed to a pore filling effect and to the increase in mass of hydrocarbons that are adsorbed on the grains, which decreases the apparent mass-to-volume ratio of the grains; meanwhile, the specific gravity decreased from 2.6815 to 2.4858 g/cm³, which is consistent with the mass-to-volume ratio of the crude oil being less than that of the mineral substrate.

There are also changes in the particle size distribution of the sand caused by crude oil contamination, as indicated in Table 5. The volume of coarser particles is more prevalent in OCS than in clean sand, probably because the hydrocarbons that accumulate around large particles inflated their volume, while the fraction of fine particles is reduced accordingly, which is attributed to the effect of oil-induced agglomeration binding small particles to larger ones or condensing them into clusters. The changes in grading, along with changes in absorption and specific gravity, have practical implications on the workability and mechanical properties of OCS concrete and need to be considered in concrete mix design.

TABLE IV. SPECIFIC GRAVITY AND WATER ABSORPTION OF UTILISED SAND

Term	Weight (gm)	
	Clean sand	Contaminated sand
Before drying	100	100
After drying (W1)	94.31	83.31
After submerged in water for 24 hrs= W2	102	107
Water absorption=WA==$\frac{W2-W1}{W1}$ *100	8.15%	28.43%
Mass= m (gm)	45	45
Volume= v (ml)	69.19	63.68
Density (ρ)= m/v (g/ml)	0.65	0.706
Specific gravity (g/ml)	2.6815	2.4858

TABLE V. PARTICLE SIZE DESCRIPTION

mesh	Clean sand		Contaminated sand	
	w	%	w	%
2360µm	12.13 gm	0.128	13.47 gm	0.16
1180 µm	10.53 gm	0.11	13.18 gm	0.158
600 µm	19.66 gm	0.20	19.80 gm	0.23
425 µm	18.07 gm	0.19	11.63 gm	0.139
300 µm	14.45 gm	0.15	9.87 gm	0.118
container	15.27 gm	0.16	12.59 gm	0.15
	90.11 gm		80.54 gm	

3.1.2.2 Shape and Texture Analysis

SEM imaging of the sand contaminated with oil (Fig. 4) shows that there is a wide range of particle sizes with representative particles measuring 550.762 µm, 344.891 µm and 396.187 µm. Particles are not only angular but also rounded; angular particles will provide mechanical interlocking and an increase in internal friction during mixing while rounded particles will have better workability but reduce the interparticle cohesiveness. Surface texture is also a factor as it can be rough or smooth, with rough surfaces encouraging adhesion between grains and cement paste and so help to make a concrete durable. These morphological properties directly affect the grading, workability and mechanical properties of OCS-based concrete.

Fig. 4. SEM images

3.1.3 Chemical Properties

3.1.3.1 Oil Content Measurement

The crude oil used for the contamination was from Al-Kut refinery, Iraq and was used at 100% concentration (undiluted). Its main properties, summarised in Table 6, are an API gravity of 25.722, a specific gravity of 0.90 at 60°F (15.6°C). The measured pH of 7.7 represents a near-neutral character with a slight alkaline trend represents a near-neutral character with a slight alkaline trend, and a pH of 7.7, it is recognised that the measurement of pH has limited interpretive value for non-aqueous materials such as crude oil.

TABLE VI. PROPERTIES OF CRUDE OIL FROM AL-KUT FIELD

Characteristic	Results
Specific Gravity @ 60 °F	0.9
API Gravity	25.722
Vapour Pressure, Reid @ 100 °F	15.0 lb/in²
Kinemative Viscosity, cst @ 60 °C	55.5
Sulphur Content, wt%	0.48
Pour point, °C	-18.0
Water Content (Dean and stark), vol.%	0.58
B .S and water (centrifuge), vol.%	0.12
Carbon Residue, wt%	83.0 %
Salt Content, ppm	8000 ppm
Wax content, wt%	18.78 %

3.1.4 Environmental Suitability

3.1.4.1 Toxicity Characteristic Leaching Procedure (TCLP)

The test is used to make sure that the OCS adheres to the environmental safety standards and doesn't release harmful contaminants. This test is used to evaluate the potential danger of waste for release of toxic elements into the environment. The intent is to identify if it is hazardous material and to quantify the amount of toxic materials present in the waste that may be released under conditions similar to those found in nature. When the concentration of toxic substances is higher than the limits that are recommended by the environmental regulations, then the waste is labelled hazardous. If the concentrations are within the permissible limits, the waste can be considered non-hazardous.

3.1.4.2 Heavy Metal Analysis

The concentrations of the various heavy metals present in the oil-contaminated sand (Table 7) showed that the heavy metals present, namely chromium (0.57 ppm), lead (0.1 ppm), nickel (0.089 ppm) and mercury (0.03 ppm) were generally low, while aluminium was not detected. The metals at these levels will not likely strongly affect the performance of concrete, but when using concrete in sensitive environments, such as those that are near water bodies, in wet and/or leaching conditions, or for long-term exposure, the presence of the metals at these concentrations may create a need for concern for ecological effects from trace metal migration.

TABLE VII. HEAVY METAL ELEMENTS

Element	Symbol	Actual Conc. [ppm]	Remarks
Chromium	Cr	0.57 ppm	Chromium is present in relatively low concentrations, but may affect the reaction with cement because chromium compounds can be harmful at higher concentrations.
Mercury	Hg	0.03	Mercury is present in trace levels. Even in small amounts, it can be had toxic effect, so it should be handled with care.
Nickel	Ni	0.089	Nickel level is very low, but it can accumulate in the environment and it may affect the long-term durability of concrete.
Aluminum	Al	Not detected	The absence of aluminium may reduce some adverse reactions.
Lead	Pb	0.1	Lead is detected in low concentration, but it may affect the surrounding environment if a leak occurs.

3.1.5 Microstructural Analysis

3.1.5.1 SEM

The microstructure of OCS particles, such as porosity and surface characteristics, were investigated using SEM in the present study. In order to achieve this objective, the SEM photographs of clean and contaminated sands by oil with various magnifications (300x, 1000x, 5000x, 20000x) are shown in Fig. 5. The microstructures of clean sand are more open, and sharp grain edges and clear boundaries are present. Oil contamination creates hazes around the grain boundaries and can allow for possible agglomeration. The presence of oil seems to affect the particle surfaces and can result in partial agglomeration of grains, resulting in the loss of a distinct microstructural boundary. More noticeable at the lower magnifications (300x – 600x). The clean sand particles seem to have a well-defined and distinct structure with clearly seen pores and voids in the particles at lower magnifications (300x - 1300x). The particles appear to have a sharp edge and seem to have irregularities on their surfaces. The other hands, the sand contaminated with the oil has lower porosity. Oil on the sand surface seems to cover some of the pores and voids. This effect is more prominent at higher magnifications (2500x-10000x), where oil is able to fill in the smaller gaps and smooth out the irregularities on the surface. Over time, the porosity is decreased by oil filling voids and micro-cracks. A clean sand surface is rough, granular, well-defined surfaces and micro projections and cracks are evident. This is a natural weathered roughness, which may be due to their original mineral content and to mechanical weathering of the sand grains. The shiny, smoother look of the oil-covered sand is due to the oil coating effect. Under higher magnifications (10000x-20000x), the layer of oil may appear as a thin film or a bridge over small cracks, which decreases the sand's roughness and granularity.

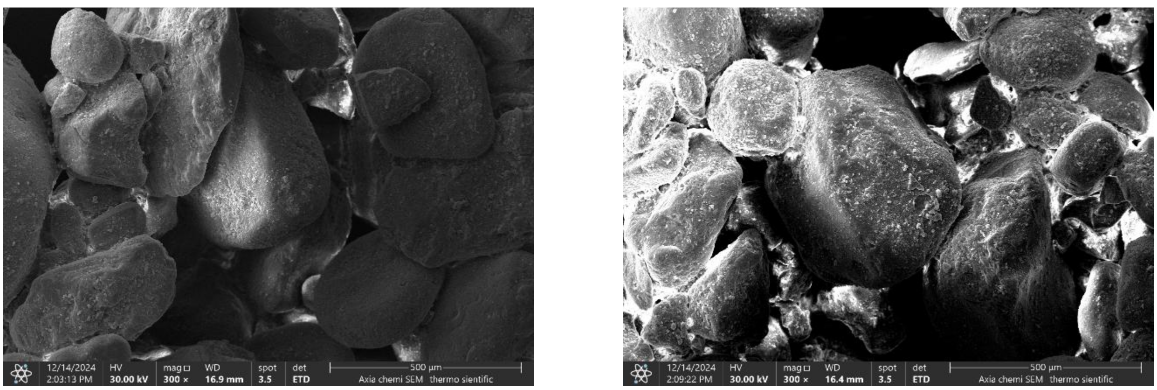

(a)

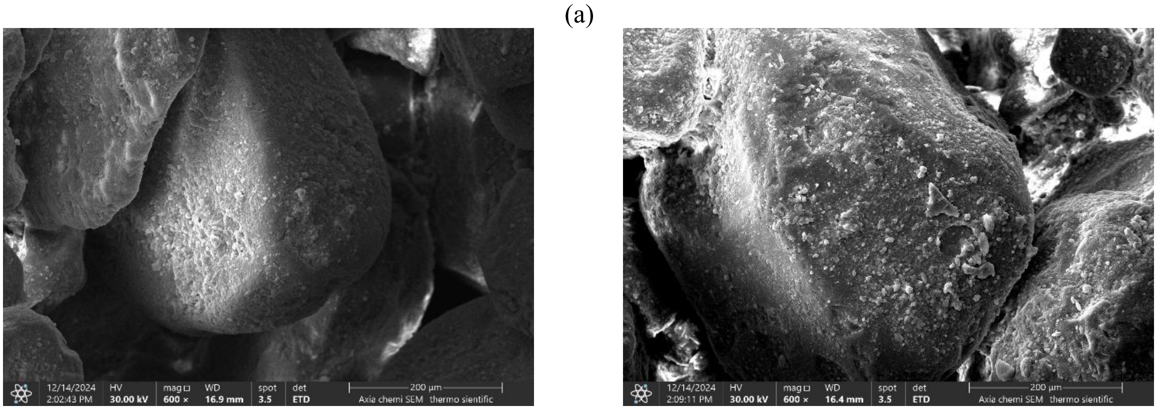

(b)

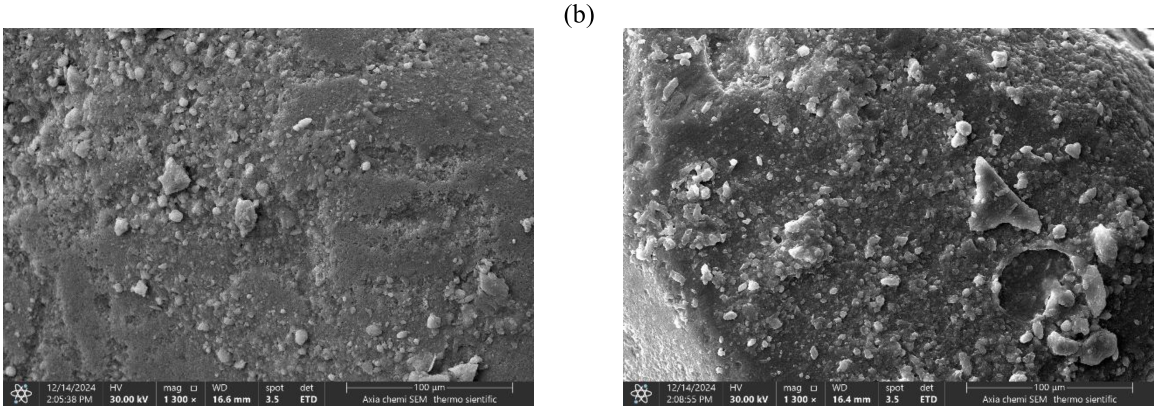

(c)

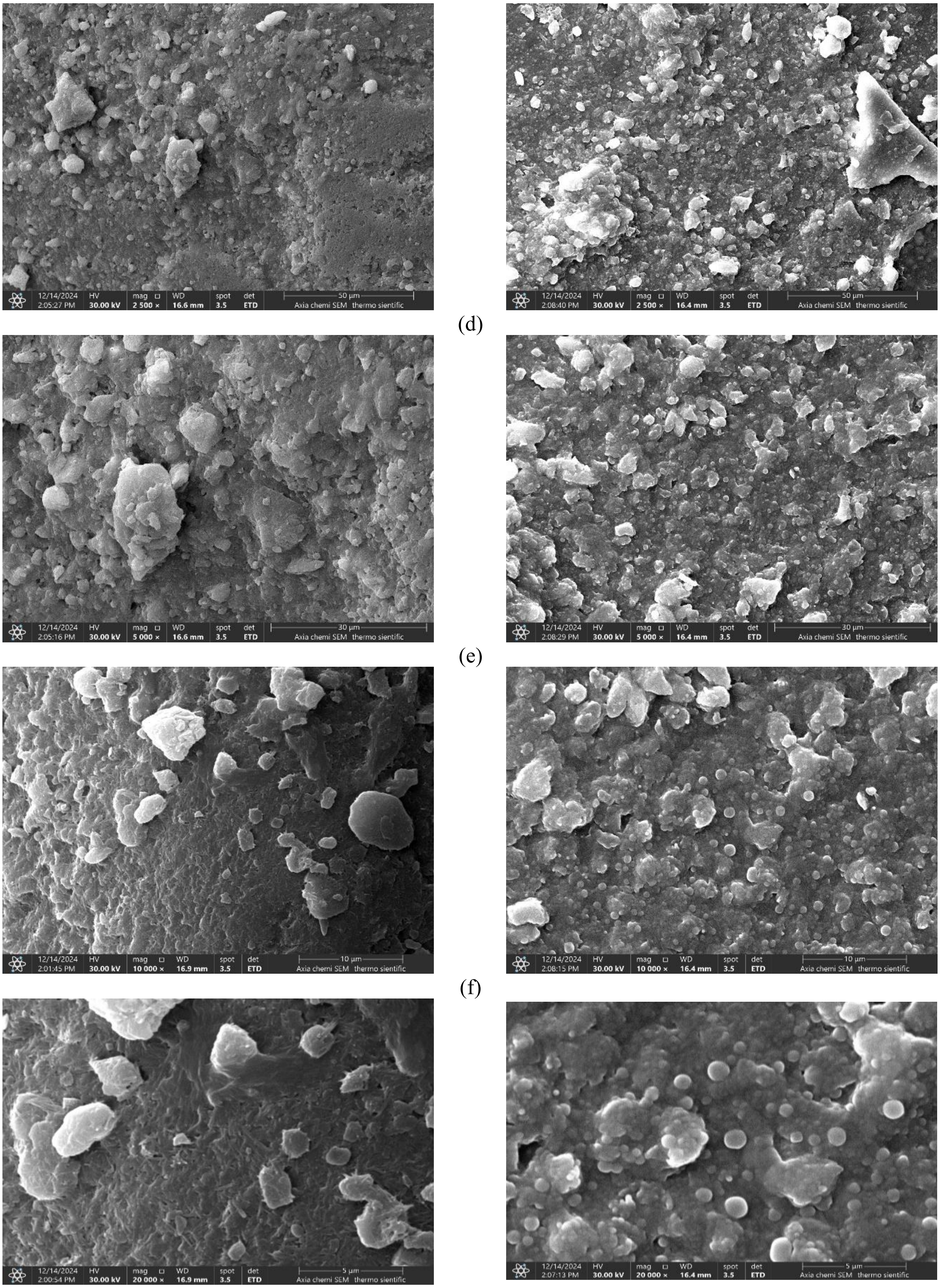

Fig. 5. SEM magnification images for clean sand (left column) and contaminated sand (right column): (a) 300X, (b) 600X, (c) 1,300X, (d) 2,500X , (e) 5,000X, (f) 10,000X, and (g) 20,000X

3.1.5.2 XRD

The XRD patterns of both clean and oil-contaminated sand sample are shown in Fig. 6. The dominant mineral in both types of sand is quartz (SiO_2) which exhibits a major peak at 2θ of approximately 26.8° (d of ≈ 3.32 Å). This peak shifts slightly to 26.96° (d = 3.3046 Å) and the intensity drops significantly, from 7,264 counts in clean sand to 2,940 counts, suggesting that the oil coating weakens the diffraction peak and causes some lattice distortion. The results of crystallite size analysis support this interpretation: contaminating the quartz decreases the dominant quartz crystallite size from 928 Å to 851 Å, and causes an increase in microstrain from 0.1789% to 0.1941%, indicating some structural disorder caused by hydrocarbon adsorption on the surfaces of the grains. The basic mineralogical makeup is preserved, but the oil changes the structure of the quartz crystals, affecting the XRD signature and implications for surface reactivity and cement–aggregate bonding.

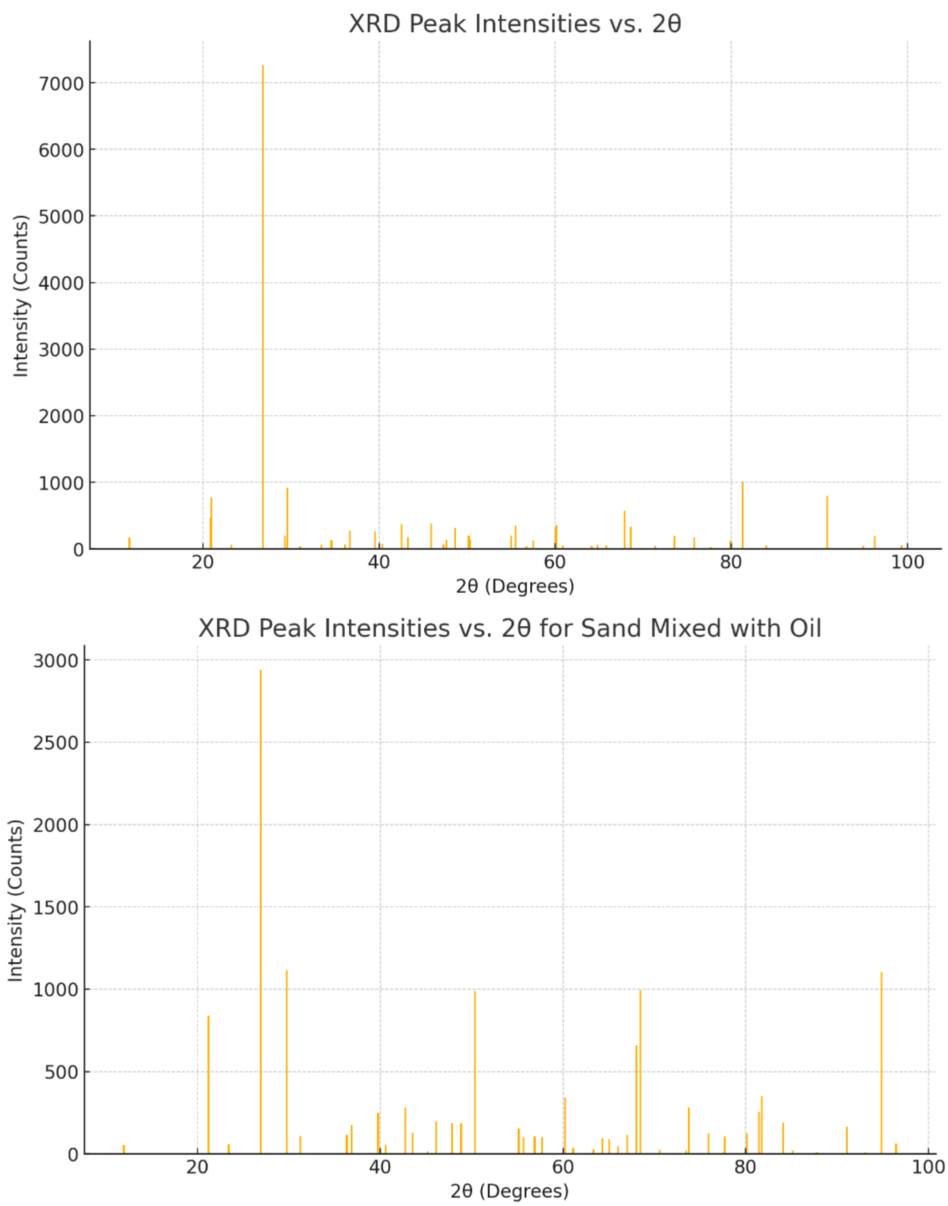

Fig. 6. XRD

3.1.5.3 Energy Dispersive X-Ray Spectroscopy (EDS)

Elemental composition of sand is measurably affected by oil contamination (Table 8 and Fig. 7) and this is confirmed by EDS analysis. Clean sand is characterised as having a high level of Oxygen (63.5), which is typical of Silicate mineralogy, as well as silicon (3.8) and low levels of Magnesium, Aluminium and Calcium. The sand samples show a decrease in Oxygen from 61.4 to 51.7, and an increase in carbon from 19.5 to 20.1, indicating the addition of hydrocarbon molecules, and increases in carbon weight percentage to 13.6%, confirming the organic contribution of the crude oil in the contaminated sand. The number of other elements, such as potassium and chlorine, are also very high in the contaminated sample and none were found in the clean sand, possibly from oil associated additives or co-contaminants. The changes in the elemental signature show that oil incorporation affects mineralogical purity of the sand and contributes a pervasive organic grain-surface phase.

TABLE VIII. EDS ELEMENT DETAILS FOR CLEAN AND CONTAMINATED SAND

Type	Element	Atomic %		Atomic % Error		Weight %		Weight % Error	
		Clean	Contaminated	Clean	Contaminated	Clean	Contaminated	Clean	Contaminated
Dominant	O	63.5	61.4	0.4	0.4	56.9	56	0.4	0.4
	Ca	5.6	0.6	0	0	12.6	1.3	0.1	0
	Si	3.8	14.4	0	0.1	6	23.1	0.1	0.1
	Mg	5.4	1	0	0	7.3	1.3	0.1	0
Minor	Al	1.5	0.9	0	0	2.3	1.4	0.1	0
	C	19.5	20.1	0.3	0.5	13.2	13.8	0.2	0.3
	S	0.4	0.4	0	0	0.7	0.8	0	0
	Fe	0.3	0.2	0	0	0.9	0.5	0	0.1
Absent	Na	-	0.6	-	0.1	-	0.8	-	0.1
	Cl	-	0.3	-	0	-	0.7	-	0
	K	-	0.1	-	0	-	0.2	-	0

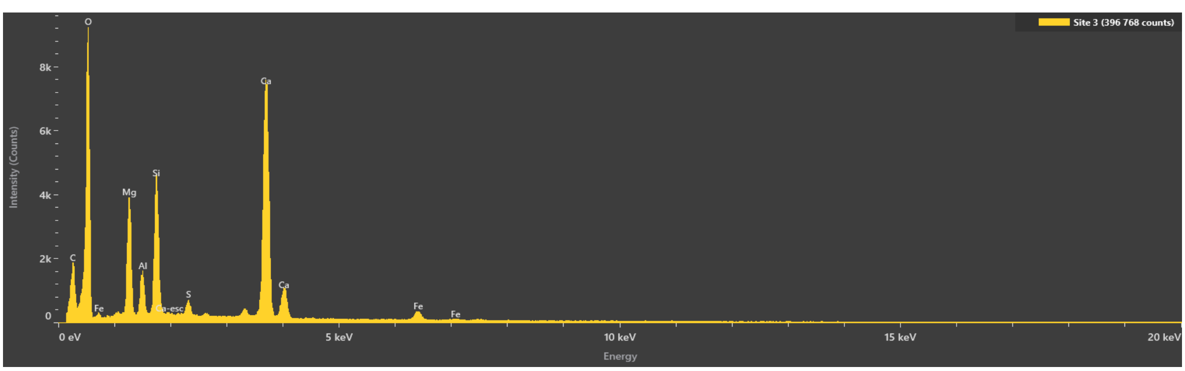

(a)

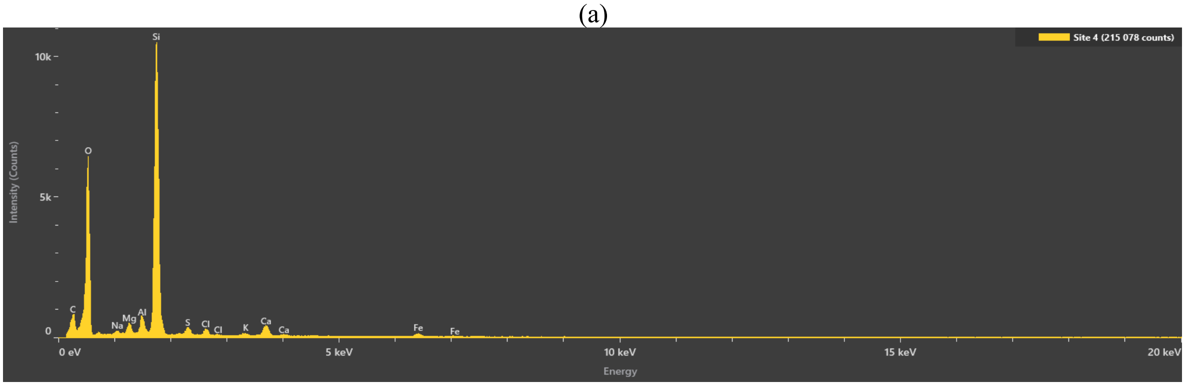

(b)

Fig. 7. EDS description for (a) Clean sand and (b) OCS

3.2 Concrete Mix Design and Specimen Programme

Concrete mix proportions were established through a systematic trial-and-error procedure targeting the desired compressive strength and mechanical properties, with full mix details provided in Table 8. Contaminated fine aggregate was prepared by blending dry sand manually with crude oil.

The sand was contaminated by blending crude oil at the target percentage of dry sand weight in a mechanical mixer, after which the contaminated sand was sealed and conditioned before batching to allow uniform absorption. The mixing water was kept constant across all mixes, and no chemical admixtures were used. The experimental programme comprised two categories of specimens (Table 9). The first consisted of 48 concrete cylinders (150 × 300 mm), 3 replicates per contamination level per age) cast at 16 oil contamination levels (0%, 2%, 4%, 6%, 8%, 10%, 12%, 14%, 16%, 18%, 20%, 22%, 24%, 26%, 28%, 30%) to characterise mechanical properties at 28 days. 30% representing the saturation limit beyond which excess oil drains freely and compromises test reliability. The oil–sand blend was sealed in a plastic container for 72 hours to ensure homogeneity and prevent evaporation before incorporation into the concrete mix. Fresh concrete was evaluated by slump test; three 150 × 300 mm cylinder specimens were then cast per batch, cured in a saturated lime-water tank, and tested at 28 days, with the reported compressive strength taken as the average of the three readings.

The second category comprised six RC beam (Fig. 8) specimens (150 × 300 × 1200 mm) incorporating OCS at contamination levels of 0%, 4%, 8%, 12%, 16%, and 20%, designed in accordance with ACI 318-19 with a reinforcement ratio of approximately 1% (2Φ10 mm bars at both top and bottom, Φ10 mm stirrups at 100 mm spacing), with steel yield strength fixed at 410 MPa.

As seen in Fig. 9, all beams were cast from the same base concrete mixture, with the only variable being the oil contamination level of the fine aggregate. After formwork removal, all specimens were moist-cured for 28 days. Beams were painted white after demoulding to aid visual crack detection during testing, then tested under two-point monotonic loading on a simply supported span of 1100 mm with load applied incrementally until failure, and used to evaluate structural performance and validate the ABAQUS finite element model.

The suggested specimens were tested with five major constant parameters:

- All dimensions for beam's sections are fixed (Depth= 300mm and width= 150mm).
- All beams have a fixed length (L=1100 mm).
- Same concrete mix.
- All beams have constant steel yield stress (f_y=410 MPa) and constant steel reinforcement ratio.
- All oil crude materials should be having the same chemical & physical properties.

And major varies parameters suggested to be studied in the proposed research:

- A varies sand oil-crude contamination ratios (0-30%).
- Apply ultimate vertical two points, where this load will be increased gradually until the failure has been seen/noted.

Each beam was tested under monotonic four-point loading using a hydraulic universal testing machine with a capacity of 2000 kN, applying load at a rate of 10 kN/min until failure. Beams were simply supported with a clear span of 900 mm. Midspan vertical deflection was measured continuously using LVDTs with 0.01 mm sensitivity, positioned at the midspan and quarter-span locations along the beam soffit. Steel reinforcement strains were measured using electrical resistance strain gauges (type KC-70-120-A1-11; 5 mm gauge length; 119.8 ± 0.2 Ω resistance) bonded to the longitudinal bars at the midspan and support regions. Concrete surface strains in the compression zone were measured using 67 mm surface-mounted gauges (119.8 ± 0.2 Ω). Load was applied monotonically at 10 kN/min via a hydraulic load cell at the beam midpoint, with all deflection, strain, and load data acquired automatically through the hydraulic machine computer and TDS-530 data logger and using an NI data acquisition system and LabVIEW software. Loading was paused at selected increments to mark and photograph crack progression, then resumed until failure. Cracking patterns and failure modes were documented photographically at each load increment. The principal outcomes recorded were load–deflection response, strain profiles, crack patterns, and failure modes.

TABLE IX. VARIABLE CONCRETE MIXTURE PROPORTIONS

Designation	ID	Fine aggregate (kg/m^3)	Oil crude (%)	Oil crude (kg/m^3)	Coarse aggregate (kg/m^3)	Cement (kg/m^3)	Water (kg/m^3)
Concrete cylinders	CS-0 (R)	756	0	0	1134	400	160
	CS-2	740.88	2	15.12	1134	400	160
	CS -4	725.76	4	30.24	1134	400	160
	CS -6	710.64	6	45.36	1134	400	160
	CS -8	695.52	8	60.48	1134	400	160

Designation	ID	Fine aggregate (kg/m^3)	Oil crude		Coarse aggregate (kg/m^3)	Cement (kg/m^3)	Water (kg/m^3)
			(%)	(kg/m^3)			
	CS -10	680.4	10	75.6	1134	400	160
	CS -12	665.28	12	90.72	1134	400	160
	CS -14	650.16	14	105.84	1134	400	160
	CS -16	635.04	16	120.96	1134	400	160
	CS -18	619.92	18	136.08	1134	400	160
	CS -20	604.8	20	151.2	1134	400	160
	CS -22	589.68	22	166.32	1134	400	160
	CS -24	574.56	24	181.44	1134	400	160
	CS -26	559.44	26	196.56	1134	400	160
	CS -28	544.32	28	211.68	1134	400	160
	CS -30	529.2	30	226.8	1134	400	160
RC beams	RC-0 (R)	756	0	0	1134	400	160
	RC-4	725.76	4	30.24	1134	400	160
	RC-8	695.52	8	60.48	1134	400	160
	RC-12	665.28	12	90.72	1134	400	160
	RC-16	635.04	16	120.96	1134	400	160
	RC-20	604.8	20	151.2	1134	400	160

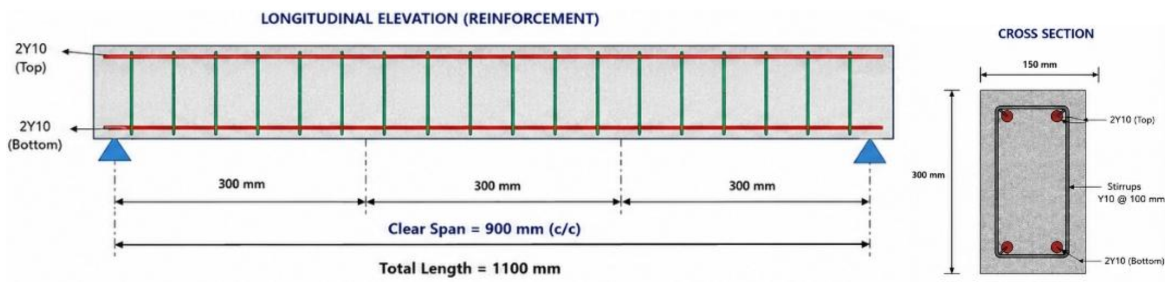

Fig. 8. Geometrical sections

Fig. 9. Preparation details for casting the RC beams.

3.3 Numerical Modelling

3.3.1 Model Construction

The nonlinear RC beam model was developed in ABAQUS 2021 (Fig. 10) using a 3D deformable solid for the concrete beam geometry (150 × 300 × 1200 mm), with concrete behaviour defined through the Concrete Damaged Plasticity (CDP) model incorporating elastic modulus, compressive stress–strain, tensile behaviour, and damage parameters. Steel reinforcement was modelled as wire elements (T3D2) with an elastic–plastic material definition and embedded into the concrete using the Embedded Region constraint. A Static, General step with NLGEOM = ON was adopted, boundary conditions replicated simple support conditions (one pinned, one roller), and two-point loading was applied as displacement-controlled loading at the designated points. Concrete was meshed using C3D8R elements with refinement at midspan and loading zones, and the load–deflection response was extracted at the midspan node and compared against experimental results, with tension stiffening and damage parameters iteratively adjusted until satisfactory agreement was achieved. The Dilation angle (ψ), eccentricity (ε), Biaxial/uniaxial strength ratio, (f_{b0}/f_{c0}), Deviatoric shape factor (Kc), and Viscosity parameter (μ) are 40° , 0.1, 1.16, 0.667, and 0.0001, respectively.

Prior to the full simulation programme, a mesh sensitivity study was conducted on the control beam RC-0 (Fig. 11), characterised by a compressive strength of 38.43 MPa, cross-section of 150 × 300 mm, and reinforcement of 2Φ10 top and bottom with Φ10 stirrups at 100 mm spacing. Four mesh configurations were evaluated (Fig. 12), starting from a coarse 40 mm seed size and progressively refined. The results confirmed that solution convergence was achieved at a seed size of 20 mm (Fig. 12), beyond which further refinement produced no appreciable change in the predicted load–deflection response. To maintain the numerical balance, accuracy, and efficiency, this mesh density was adopted.

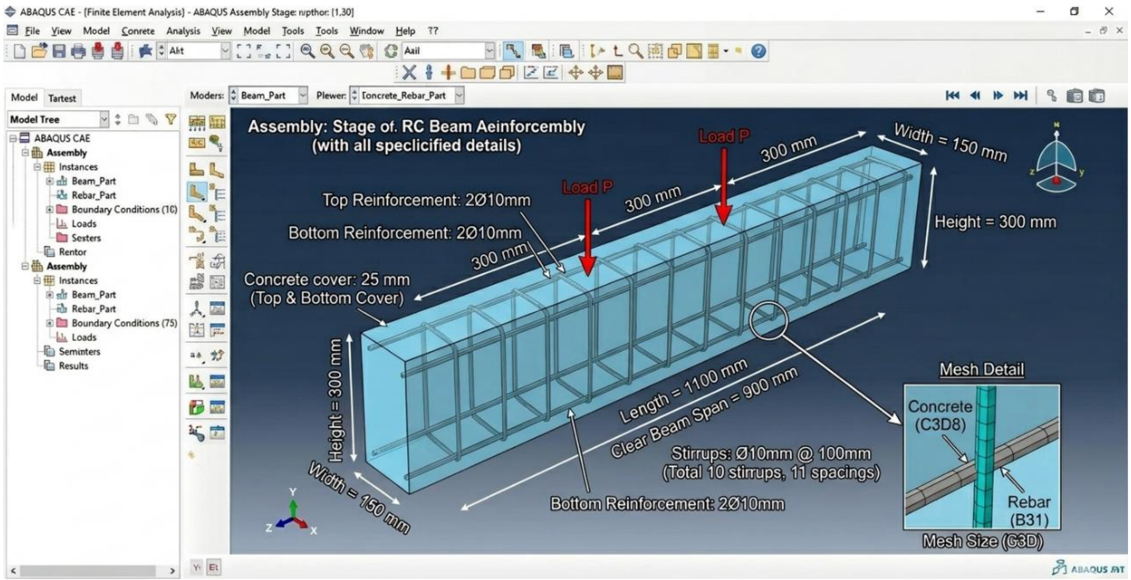

Fig. 10. Constructing RC beam in FEM

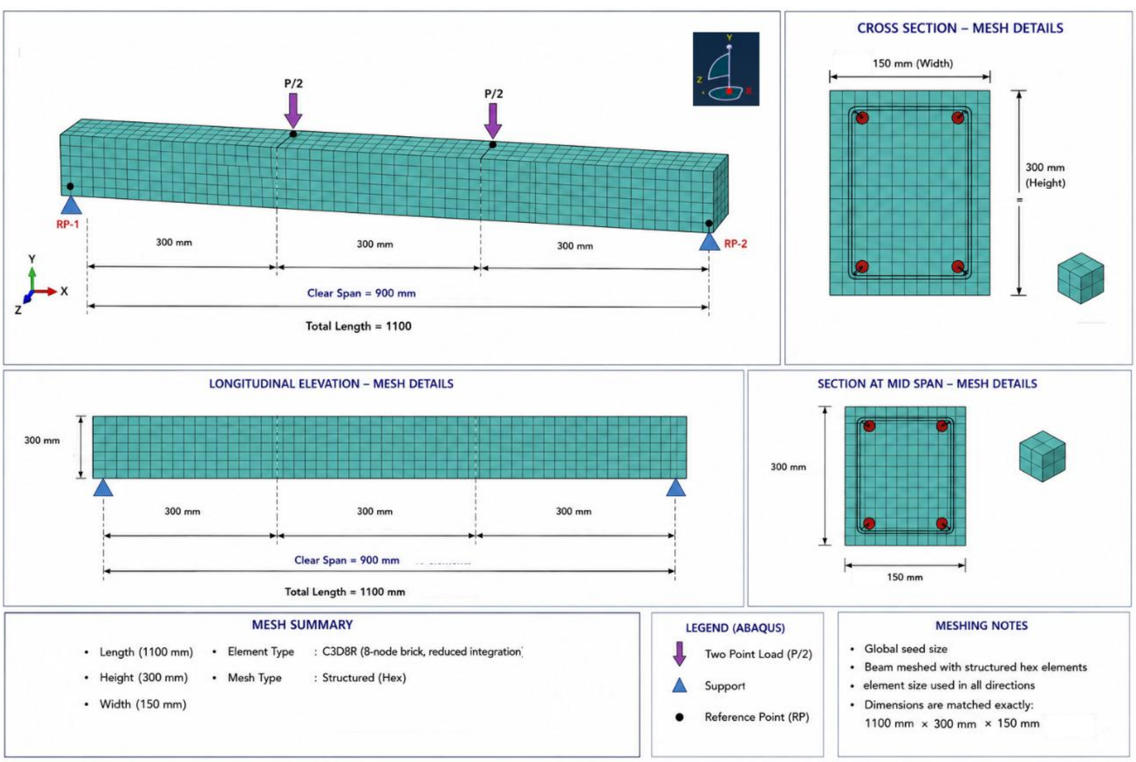

Fig. 11. FEM Meshing

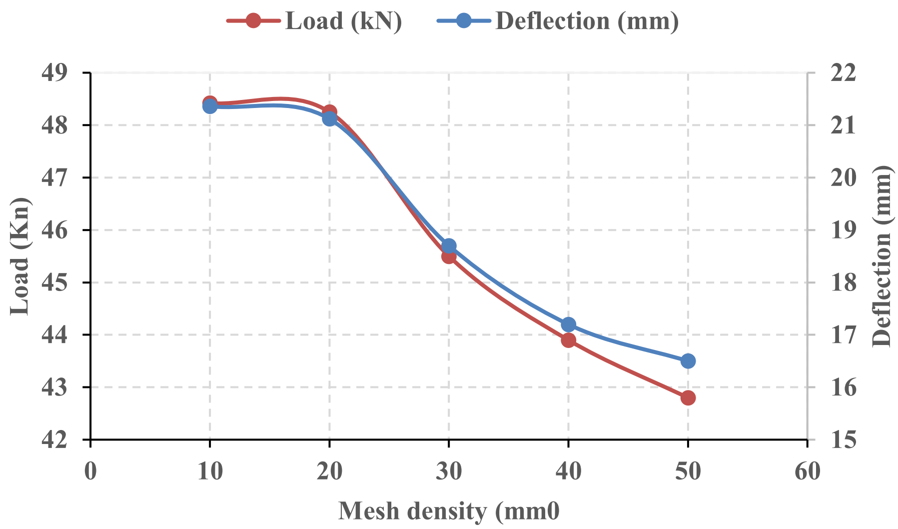

Fig. 12. Mesh size accuracy

3.3.2 Parametric Study

Following successful validation, the calibrated ABAQUS model was used to conduct a systematic parametric study examining the sensitivity of structural performance to five variables (Table 10): concrete compressive strength, stirrup spacing, beam clear span, boundary conditions, and contamination level beyond the experimental range. All runs used a reference configuration of 38.43 MPa compressive strength, 100 mm stirrup spacing, 900 mm clear span, simply supported conditions, and 20% oil content, the latter retained as the baseline for geometric and material parameter runs because it represents the most severely compromised contamination state and is therefore the most practically relevant context for evaluating mitigation measures. Each parameter was varied independently while all others remained fixed.

TABLE X. PARAMETRIC STUDY

No.	Parameters	Values	Reason
1.	Strength (*f'c*)	30 MPa	To investigate the influence of concrete strength on load capacity,
		38.43 MPa	
		50 MPa	
2.	Bar spacing	75 mm	To study its effect on flexural and shear performance.
		100 mm	
		150 mm	
		200 mm	
3	Clear span	750	To evaluate the influence of span-to-depth ratio on structural behaviour.
		900	
		1200	
4	Boundary Conditions	Simply Supported	To assess stress distribution and deformation patterns.
		Fixed-Pinned	
		Fixed-Fixed	

No.	Parameters	Values	Reason
5.	Contamination Level	20%	To analyse the effect of varying levels of oil contamination in sand
		24%	
		28%	
		32%	

4. RESULTS AND DISCUSSION

This section presents and discusses the results of the experimental and numerical programmes. The experimental work is reported at two levels: at the material level, fresh and hardened concrete properties, workability, unit weight, 28-day compressive strength, splitting tensile strength, and modulus of rupture, were measured across six contamination levels (0%, 4%, 8%, 12%, 16%, and 20%); at the structural level, six RC beams designated RC-0 through RC-20 were tested under two-point monotonic loading on a 900 mm clear span, with results reported in terms of first crack load, ultimate load, midspan load–deflection response, reinforcement strain, crack propagation, and failure mode. The second part of the section addresses the nonlinear finite element analysis conducted in ABAQUS/Standard 2021, in which a three-dimensional CDP model was calibrated from measured material properties, validated against all six experimental beams using both qualitative and quantitative error metrics, and subsequently used for a parametric study covering concrete compressive strength, stirrup spacing, beam clear span, boundary conditions, and an extended contamination range of 0–32%.

4.1 Mechanical Properties of Concrete

The mechanical properties of concrete under all contamination levels are summarised in Table 11, which also shows the percentage changes with respect to the uncontaminated concrete. A consistent and characteristic behaviour is seen throughout all of the properties – an improvement which occurs at 2% oil content, corresponding to the pore-filling and particle-packing improvement when oil is added, and a progressive and non-linear deterioration at higher oil content.

TABLE XI. FRESH AND HARDENED PROPERTIES

Property	0%	2%	4%	6%	8%	10%	12%	14%	16%	18%	20%	22%	24%	26%	28%	30%
Fd (kg/m³)	2440	2430	2370	2350	2320	2300	2280	2260	2240	2220	2200	2180	2160	2140	2120	2100
Fd (%)	0	-0.41	-2.87	-3.69	-4.92	-5.74	-6.56	-7.38	-8.20	-9.02	-9.84	-10.66	-11.48	-12.30	-13.11	-13.93
Dd (kg/m³)	2439.5	2420	2340	2320	2290	2280	2260	2240	2220	2200	2180	2160	2140	2120	2100	2080
Dd (%)	0	-0.80	-4.08	-4.90	-6.13	-6.54	-7.36	-8.18	-9.00	-9.82	-10.64	-11.46	-12.28	-13.10	-13.92	-14.74
f'c (MPa)	38.43	39.21	36.51	33.82	31.14	28.45	25.77	23.08	20.4	17.71	15.03	14.26	13.49	12.72	11.95	11.18
f'c (%)	0	2.03	-5.00	-12.00	-18.97	-25.97	-32.94	-39.94	-46.92	-53.92	-60.89	-62.89	-64.90	-66.90	-68.90	-70.91
ft (MPa)	3.48	3.52	3.31	3.06	2.78	2.43	2.09	1.74	1.39	1.04	0.70	0.63	0.56	0.49	0.42	0.35
ft (%)	0.00	1.15	-4.89	-12.07	-20.11	-30.17	-39.94	-50.00	-60.06	-70.11	-79.89	-81.90	-83.91	-85.92	-87.93	-89.94
fr (MPa)	3.85	3.89	3.66	3.39	3.12	2.85	2.58	2.31	2.04	1.77	1.50	1.42	1.34	1.26	1.18	1.10
fr (%)	0.00	1.04	-4.94	-11.95	-18.96	-25.97	-32.99	-40.00	-47.01	-54.03	-61.04	-63.12	-65.19	-67.27	-69.35	-71.43
Ec (GPa)	29.35	29.63	28.18	27.00	25.82	24.64	23.46	22.28	21.10	19.92	18.74	18.23	17.72	17.21	16.70	16.19

Property	0%	2%	4%	6%	8%	10%	12%	14%	16%	18%	20%	22%	24%	26%	28%	30%
Ec (%)	0.00	0.95	-3.99	-8.01	-12.03	-16.05	-20.07	-24.09	-28.11	-32.13	-36.15	-37.89	-39.63	-41.36	-43.10	-44.84

4.1.1 Fresh and Dry Density

Fresh density decreased continuously from 2440 kg/m³ (0% oil) to 2100 kg/m³ (30% oil), a reduction of 13.93%. Reductions in dry density were always larger than in fresh density, reducing from 2439.5 to 2080 (14.74% at 30%) (Fig. 13). The higher relative decrease of dry compared to fresh density is a sign of the lasting disruption of the microstructures caused by the presence of oil in the fresh state, which is partially displaced during mixing and consolidation, but also chemically affects the formation of C–S–H gels after hardening, leading to a more porous but less dense matrix.

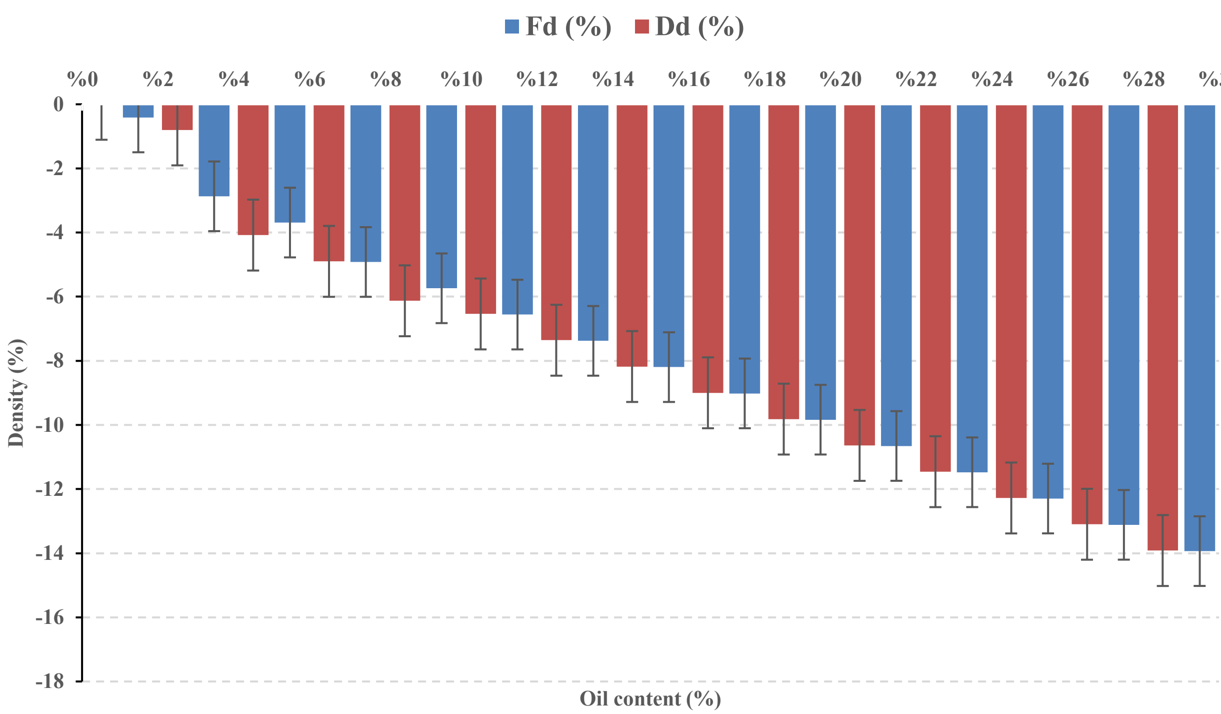

Fig. 13. Densities (%) vs. oil content (%)

4.1.2 Compressive Strength

As shown in Fig. 14, the compressive strength of the packing was found to improve slightly by 2.03% when the oil content was 2% ($f'c$ = 39.21 MPa), which agrees with the light crude oil optimum cohesion value of fine sand packing reported by some researchers [11]. After this peak, strength drops off gradually and non-linearly. The reduction of $f'c$ is 25.97% to 28.45 MPa at 10% contamination and 60.89% to 15.03 MPa at 20% contamination, which is less than the typical requirement for structural concrete. The 30% contaminated sample gives a value of $f'c$ equal to 11.18 MPa which is a 70.91% reduction. This deterioration is thought to be caused by the formation of oil films around aggregate particles which inhibits direct chemical bonding between the cement paste and the aggregates, and as the oil is progressively displaced during hydration and drying, the void content increases and the ITZ weakens.

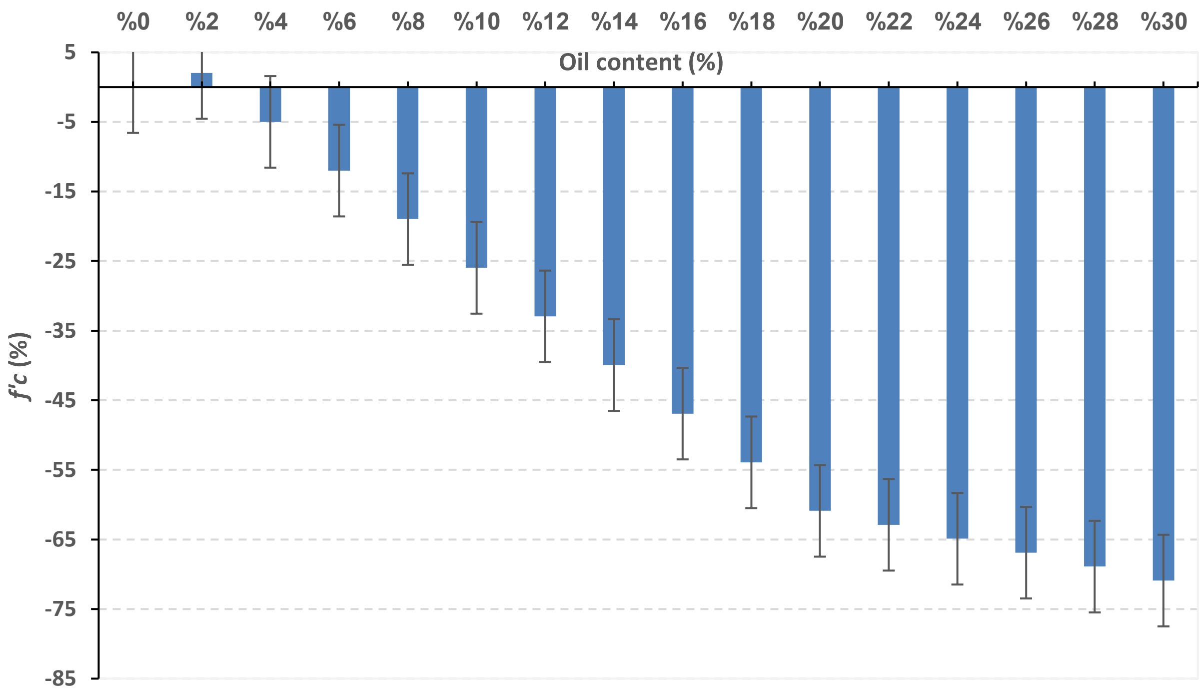

Fig. 14. Compressive strength

4.1.3 Splitting Tensile Strength

The tensile strength is the most sensitive property tested to the presence of oil. Following a marginal 1.15% increase at 2% oil, ft decreases to −20.11% at 8%, −50.00% at 14%, −79.89% at 20%, and −89.94% at 30% oil content (Fig. 15). The increased sensitivity compared to compressive strength is the result of this sensitivity affecting tensile failure, namely with respect to the initiation and propagation of cracks along the weakest interfaces in the concrete structure, which are the oil-contaminated ITZ zones. Compressive loading can close cracks and may also redistribute stresses throughout the matrix, even if it has been partially degraded by the impact of the cracks; however, tensile loading takes advantage of the weaknesses of the interfaces. The sharp drop where oil content is less than 10–14% is due to a change in failure modes: at these amounts of oil, the oil placed around the aggregate particles does not allow for any meaningful adhesive bond between the paste and the aggregate; instead, the failure is controlled by slippage occurring at the interface rather than by failure of the cement paste.

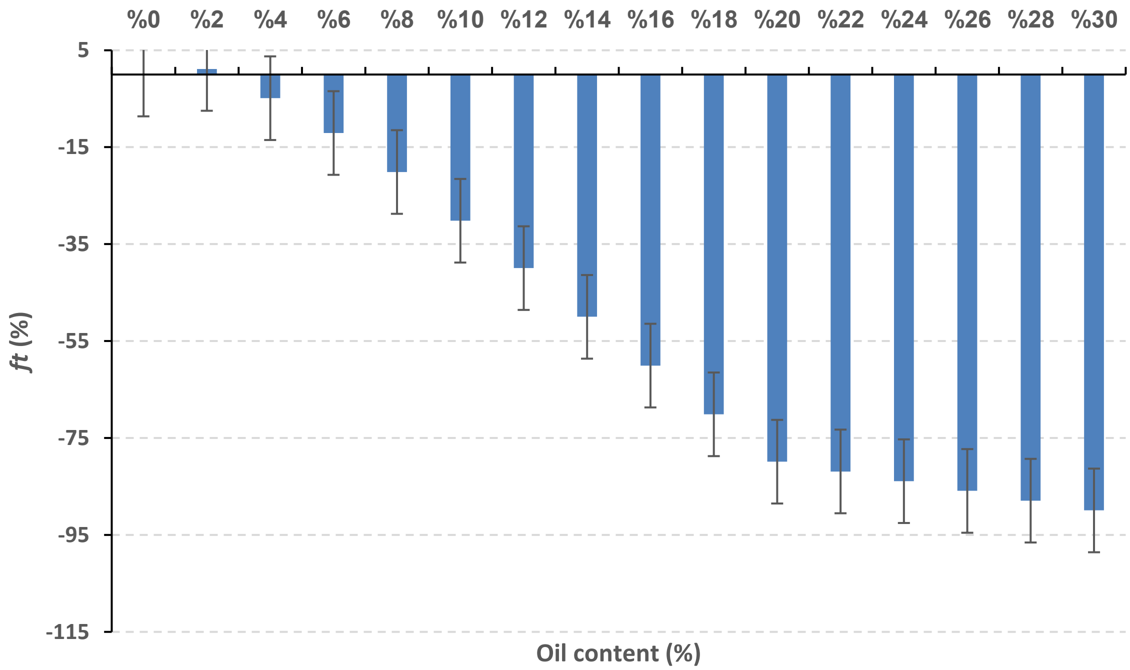

Fig. 15. Tensile strength

4.1.4 Modulus of Rupture (Flexural Strength)

The non-monotonic trend for the other mechanical properties is also evident for the modulus of rupture, with a marginal improvement of 1.04% at very low contamination (2% oil content) due to better particle packing and a marginally denser ITZ, before a gradual, continuous and steep drop with increasing oil content (Fig. 16). The reductions are at 4% at 4%, 11.95% at 6%, 25.97% at 10%, 47.01% at 16%, 61.04% at 20% and 71.43% at 30% oil content, due to the progressive disruption of cement hydration, weakening of the bond between the paste and the aggregates and increase of the entrapped void content which lessen the ability to resist tensile stresses at the extreme fibre under bending. Interestingly, the magnitude of the flexural strength loss is invariably less than the corresponding splitting tensile strength loss, which reaches 89.94% at 30%, as the flexural loading allows the stress to be redistributed across the cross section and some stress can still be carried by the remaining bond network, albeit in an impaired condition, while direct tensile loading requires a complete failure of the bond network across the full failure plane and as such is more sensitive to oil-induced microstructural deterioration.

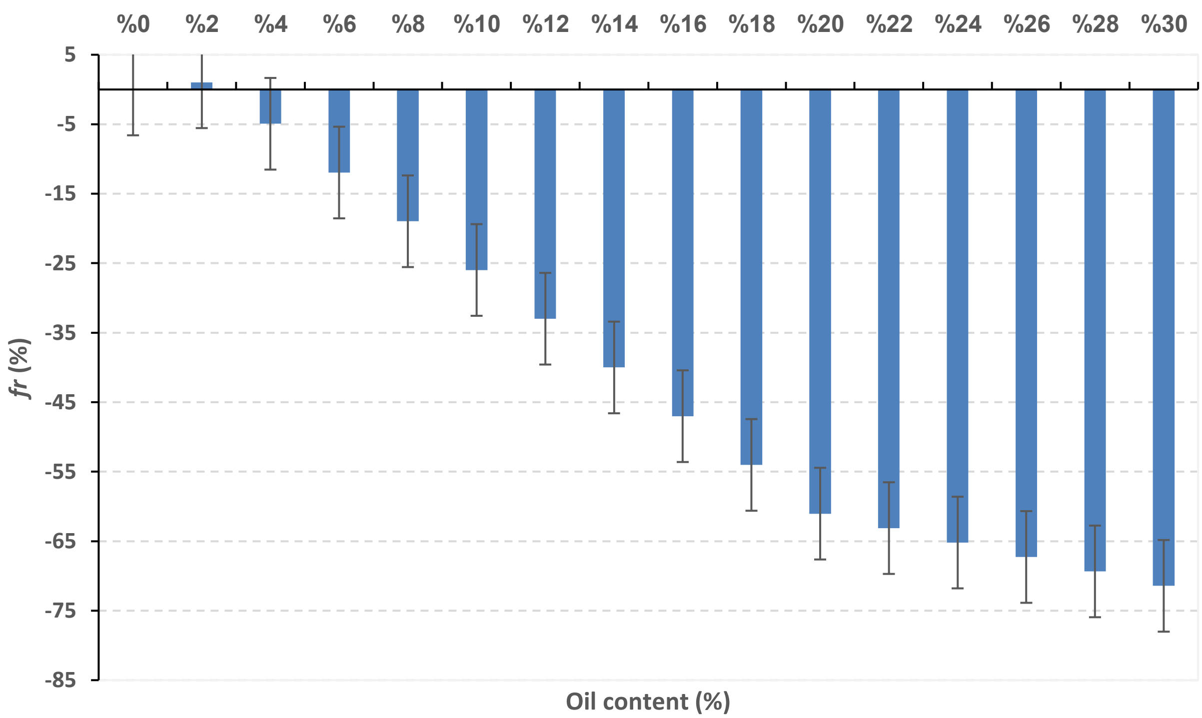

Fig. 16. Flexural strength

4.1.5 Modulus of Elasticity

The modulus of elasticity (Ec) of concrete decreases gradually with an increase in oil content (except for a marginal increase of 0.95% for 2% oil level, which is due to pore filling and slightly better particle packing at very low levels of contamination). Beyond this optimum, stiffness declines continuously: reductions reach 3.99% at 4%, 8.01% at 6%, 16.05% at 10%, 28.11% at 16%, 36.15% at 20%, and 44.84% at 30% oil content. These losses are due to the progressive degradation of the cement hydration that takes place as a result of hydrocarbon films on the aggregate surface, weakening of the interfacial transition zone (ITZ), and the formation of entrapped voids within the cementitious matrix that compromise its continuity. Because the behaviour of the concrete under service loads occurs in the elastic range, and because there are factors that can affect serviceability beyond the simple compressive or tensile strength data, the sustained reduction in Ec has implications for oil contaminated concrete that is not aligned with the reduction in compressive or tensile strength.

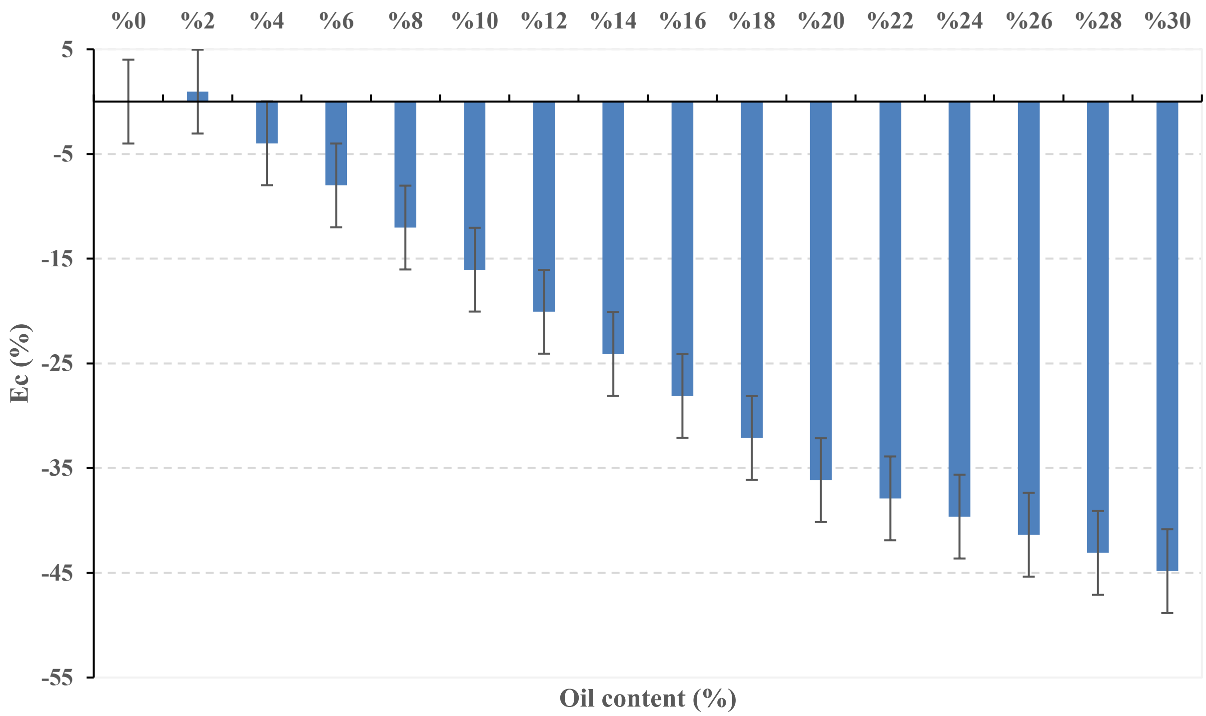

Fig. 17. Elasticity Modulus

4.2 Structural Performance of RC Beams

4.2.1 Load-Deflection

Load–deflection curves (Fig. 18 and Fig. 19) show that the structural performance deteriorates in a progressive manner with a gradual increase in oil contamination, from 0% to 20%. The control beam RC-0 shows the typical ductile flexural behaviour, followed by linear elastic, and then by a progressive decrease in stiffness after cracking and finally a wide descending branch, indicating high strength of the paste–aggregate bond and high energy absorption capacity. At higher levels of contamination (above 8% oil) all key performance indicators worsen significantly, with cracking load reduction of ≈ 33% and ultimate load of ≈ 19% occurring at the 4% oil level, indicating high level of aggregate surface coating and degradation of the ITZ. Ultimate load loss is close to 33% at 12% oil, and the deflection capacity decreases by ≈ 30%, the curve shape changing to steep and narrow, which suggests a change in the behaviour from ductile to brittle. The curves have steep ascending branches and abrupt load drops after peak, to the extent of ≈70% of the cracking load, ≈61% of the ultimate load, and ≈60% of the deflection capacity after 20% oil, when the transition becomes critical. In every contamination level, percentage reduction of cracking load is always higher than that of ultimate load, which remains the conclusion that tensile-governed properties are more sensitive to the presence of oil in the environment than the compressive capacity. These findings suggest that it is likely a contaminant concentration of 8-12% is a critical threshold for structural performance, as load capacity, ductility and energy absorption will all be affected beyond this concentration level.

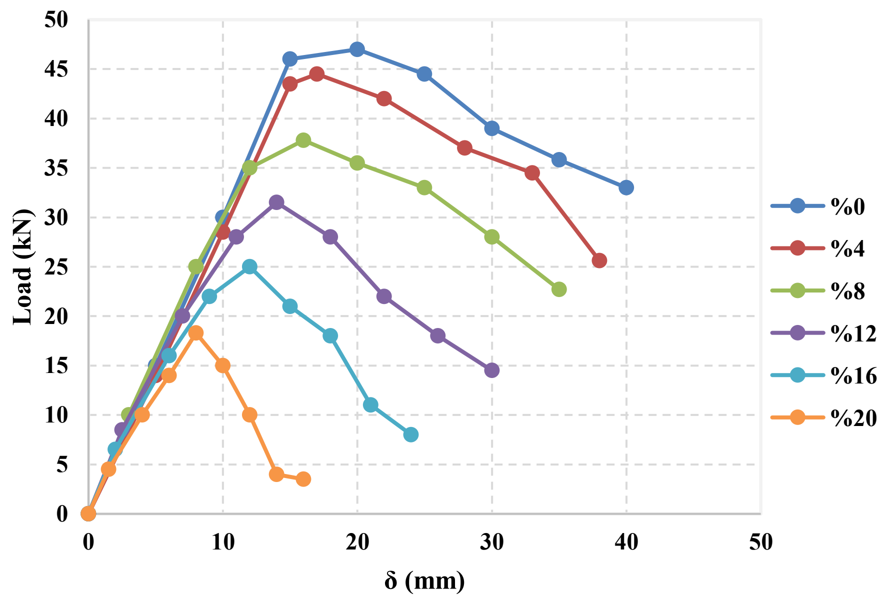

Fig. 18. Load-Deflection Curves for Beams with Varying Oil Content

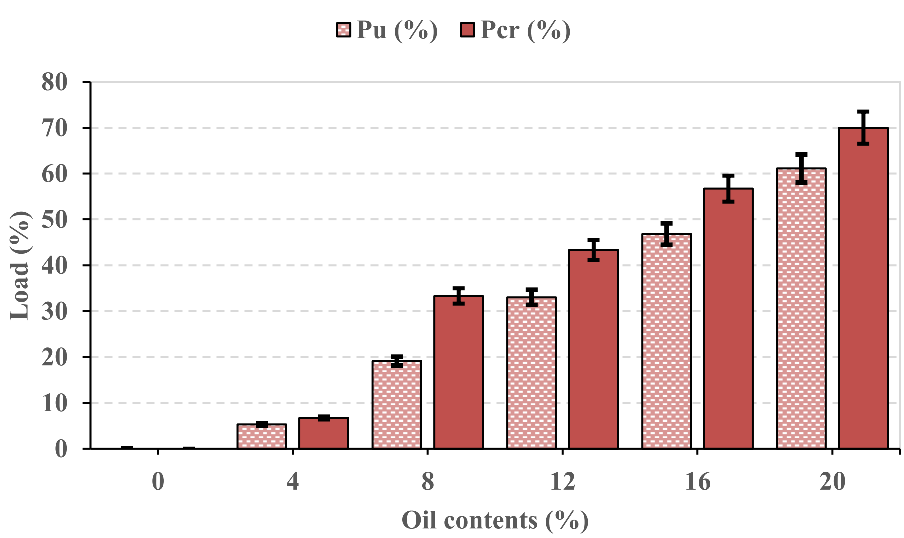

Fig. 19. Ultimate and cracking loads (%) vs. oil content (%)

4.2.2 Comparative evaluation of RC Beam with and without oil contamination

The comparative evaluation (Table 12) shows that the performance of an RC beam decreases in three different aspects of its behaviour when contaminated with crude oil, all of which are interrelated: load capacity, ductility, and energy absorption. The cracking load drops to 4.5 kN at 20% contamination level, a 70% reduction, so that when the beam is under normal service loads, it is in a state of cracking and the reinforcement is susceptible to corrosive ingress which will increase long-term deterioration. The ultimate load reductions are non-linear from 5.3% at 4% contamination up to 61.1% at 20% with a very high deterioration rate beyond 8% oil content.

The progressive ductile to brittle failure is the more structurally important effect. The control beam will exhibit a distinct plastic plateau from about 15 mm to 25 mm of deflection, giving an adequate amount of energy absorption and warning of imminent collapse. This ductility decreases with increasing contamination at 4-6% and is significantly reduced at 8% and higher, when the beams suddenly collapse with very little permanent deformation when loaded to their peak, due to the reduction in bond strength caused by oil contamination, which is not sufficient to allow the steel to develop the yield strength by transferring the bond in a progressive manner. This loss of energy absorption capacity makes contaminated concrete especially sensitive to dynamic loading conditions in which ductile dissipation is crucial. All together, these results define 8% oil contamination as a critical threshold for structural properties, below which the ability to carry load, exhibit ductility, and possess post-cracking stiffness is incompatible with safe structural performance.

The present results are consistent with, and extend, the only prior beam-scale evidence available. Abousnina et al. [11] recorded 20% ultimate-load reduction for a single beam containing 6% light crude oil (100 × 250 × 1400 mm, 2N10 bars top and bottom) while the ultimate-load reduction recorded in this study for beam RC-8 was approximately 15% and cracking load reduction was approximately 33.3% at 8% contamination (150 × 300 × 1200 mm). The differences in ultimate-load sensitivity are due to the different cross-section and reinforcement ratio of the specimen, which makes their capacity more sensitive to the loss of paste-aggregate bond as well as due to the difference in oil properties and conditioning procedure. The two studies concur with the mechanism of degradation, which is tensile- and bond-controlled prior to any loss of compressive capacity, and the present programme identifies the transition point within a systematically tested range, not at a single point as proposed here, as 8-12%.

TABLE XII. LOAD-DEFLECTION EVALUATION AT VARIOUS CONTAMINATION LEVELS

Oil Content (%)	Pcr (kN)	Pcr Reduction (%)	Pu (kN)	Pu Reduction (%)	Δ at Pu (mm)	Ductility Ratio (Approx.)	Failure Type
0	15.0	0.0	47.0	0.0	20.0	High	Ductile
4	14.0	6.7	44.5	5.3	17.0	Moderate-High	Ductile
8	10.0	33.3	38.0	19.1	16.0	Moderate-Low	Brittle
12	8.5	43.3	31.5	33.0	14.0	Low	Very Brittle
16	6.5	56.7	25.0	46.8	12.0	Very Low	Extremely Brittle
20	4.5	70.0	18.3	61.1	8.0	Negligible	Explosive

4.2.3 Load-Strain Relationship (Tension Zone)

Load–strain relationships (Fig. 20) show that systematical changes in the structural response, from ductile to brittle, are observed as a result of oil contamination. Full development of steel strain is obtained with near yield condition for the control beam in the tension zone, which is the standard for ductile flexural behaviour. The loss of maximum steel strain is still in the range of 5-15% at low contamination levels, while the beam is overall still in a very ductile state with minor decrease in post cracking stiffness. When the level of contamination gets to moderate (25-40% steel strain reduction), the steel is in incomplete yielding, tension stiffening is reduced, and composite action is partially lost. For higher levels of contamination, strain reductions are greater than 50–70% because they tend to fail prematurely, before the load is transferred to the reinforcement; there is no strain, and the load–strain curve is very short and steep. At very high contaminant concentration the strain capacity loss is greater than 70–80%, and often the structural system fails well before significant deformations have occurred, as is seen in the load-deflection response and indicates brittle failure and explosive failures. The gradual loss in the strain capacity of steel is thus also representative for the bond degradation mechanism, further confirming that the oil contamination has a negative effect not only on strength but also on the ductility and energy absorption of the steel which is fundamental for structural safety.

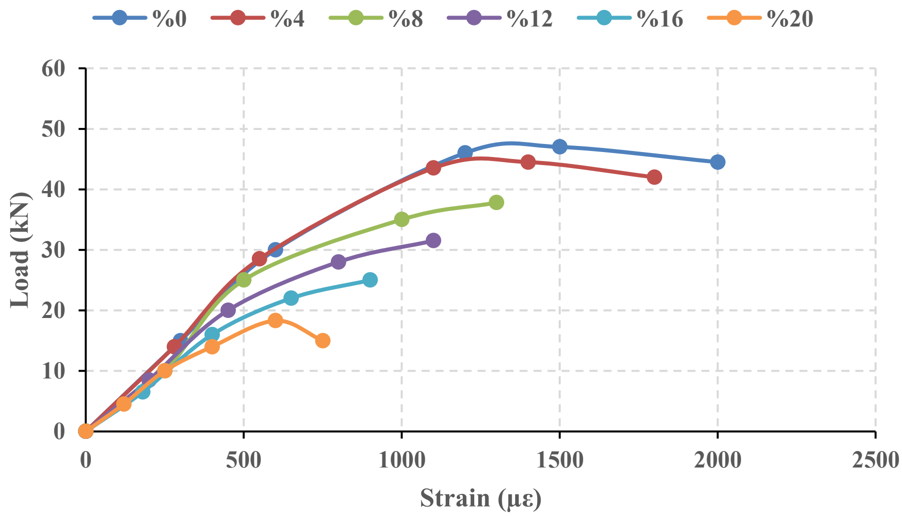

Fig. 20. Steel reinforcement strain vs. load relationship

4.2.4 Load-Strain Behaviour (Compression Zone)

The concrete load-strain response (Fig. 21) is similar, but naturally has smaller strain magnitudes because it is compression controlled. In this case the oil contamination effect can be again discussed by considering the percentage reduction in capacity of compressive strain. When a concrete is not contaminated, it reaches its full strain capacity in the elastic-nonlinear range (100% reference performance). When contamination is low, the amount of reduction in concrete strain is relatively small (5-10 %), and the compression zone still has a rather high degree of effectiveness and stability.
At intermediate contamination concentration, the reduction in the strain of the concrete is more pronounced and typically found within the range of 20-35% reduction. It is an indication of lower stiffness and compressive resistance resulting from higher porosity and less microstructure strength. The curve starts to deviate from a more linear, non-linear characteristic, thus representing a decrease in the energy absorption capacity. For higher concentrations, it is found that the compressive strain capacity is significantly reduced, sometimes by 40-60%. The concrete can no longer effectively resist the compressive stress and the development of the strain is restricted. The curves are steeper and cut off early due to early failure of the compression zone. For very high levels of contamination, the reduction can be greater than 60-70%, which means that the concrete breaks at very small strain. Important, these strains are well below the crushing strain levels typical of those for the material, making it clear that failure is not controlled by the crushing capacity of the material, but by the structural instability and degradation of the bonds.

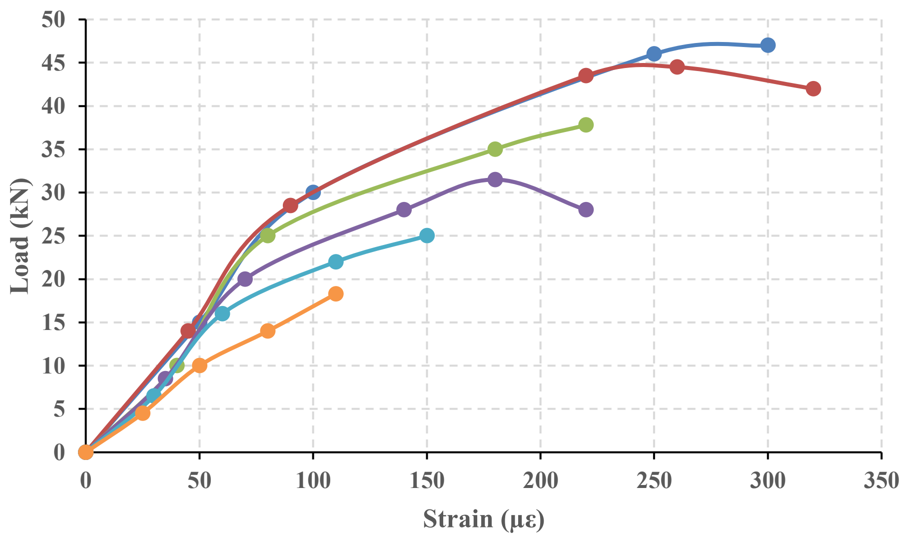

Fig. 21. Concrete strain vs. load relationship

4.3 Cracking Patterns and Failure Mode Transition

The control beam displays ductile behaviour, including multiple cracks which are well distributed vertically, beginning to form at midspan, a long plastic deformation phase between the formation of cracking (15.0 kN) and ultimate load (47.0 kN), and large deflections that indicate that steel yielding has occurred. At 4% contamination the pattern is generally retained with only some variation in the width of the cracks, reflecting some bond deterioration at an early stage, but not with much impact on the structure. Cracks begin to widen and become more irregular in cross section at about 8% oil content, and diagonal cracking appears, along with a noticeable reduction in stress redistribution. At about 8% oil content, cracks begin to widen and become more irregular in cross section, diagonal cracking appears, and a noticeable reduction in stress redistribution can be seen, which represent the beginning of the ductile-to-brittle transition. At 12%, failure is governed by a combined flexural–shear mechanism with few but wide localised cracks and a sharply reduced post-peak response (Pu = 31.5 kN at 14 mm deflection). At 16%, crack distribution collapses to a small number of dominant diagonal cracks, bond slip governs failure, and the beam reaches its peak load of 25.0 kN at only 12 mm deflection with no meaningful plastic plateau. The 20% contaminated beam fails catastrophically at 18.3 kN and 8 mm deflection through a single dominant crack accompanied by compression zone spalling, reflecting near-complete loss of composite action. The deflected shape curves (Fig. 23) corroborate these observations: maximum curvature decreases monotonically with contamination as the modulus of elasticity and bond stiffness diminish, with the RC-20 beam exhibiting a near-flat profile indicative of extreme stiffness loss and absence of ductile deformation capacity.

TABLE XIIII. COMPLETE LOAD-DEFLECTION DATA FOR ALL CONTAMINATION LEVELS

Deflection (mm)	Load (kN) @ various percentages of oil content					
	0%	4%	8%	12%	16%	20%
0.0	0.0	0.0	0.0	0.0	0.0	0.0
2.0	-	-	-	-	6.5	4.5
2.5	-	-	-	8.5	-	-
3.0	-	-	10.0	-	-	-
4.0	-	-	-	-	-	10.0
5.0	15.0	14.0	-	-	-	-
6.0	-	-	-	-	16.0	14.0
7.0	-	-	-	20.0	-	-
8.0	-	-	25.0	-	-	18.3
9.0	-	-	-	-	22.0	-
10.0	30.0	28.5	-	28.0	-	15.0
11.0	-	-	-	-	-	-
12.0	-	-	35.0	31.5	25.0	10.0
14.0	-	-	-	-	-	4.0
15.0	46.0	43.5	-	-	21.0	-

Deflection (mm)	Load (kN) @ various percentages of oil content					
	0%	4%	8%	12%	16%	20%
16.0	-	-	37.8	-	-	-
17.0	-	44.5	-	-	-	-
18.0	-	-	-	28.0	15.0	-
20.0	47.0	-	35.5	-	-	-
21.0	-	-	-	-	8.0	-
22.0	-	42.0	-	22.0	-	-
25.0	44.5	-	30.0	-	-	-
26.0	-	-	-	12.0	-	-
28.0	-	37.0	-	-	-	-
30.0	39.0	-	18.0	-	-	-
33.0	-	24.5	-	-	-	-
35.0	25.8	-	-	-	-	-
38.0	-	0.0	-	-	-	-
40.0	0.0	-	-	-	-	-

RC-0

RC-4

RC-8

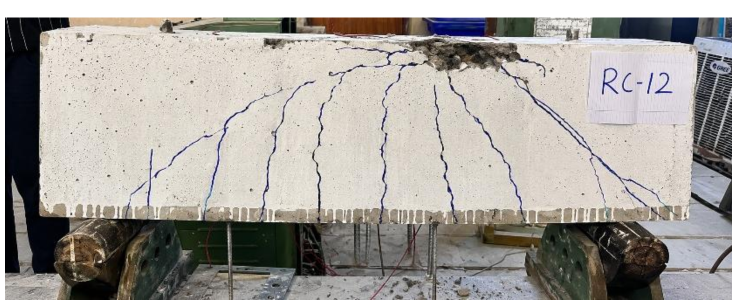

RC-12

RC-16

RC-20

Fig. 22. Photographs illustrate the failure and cracks of the RC beams

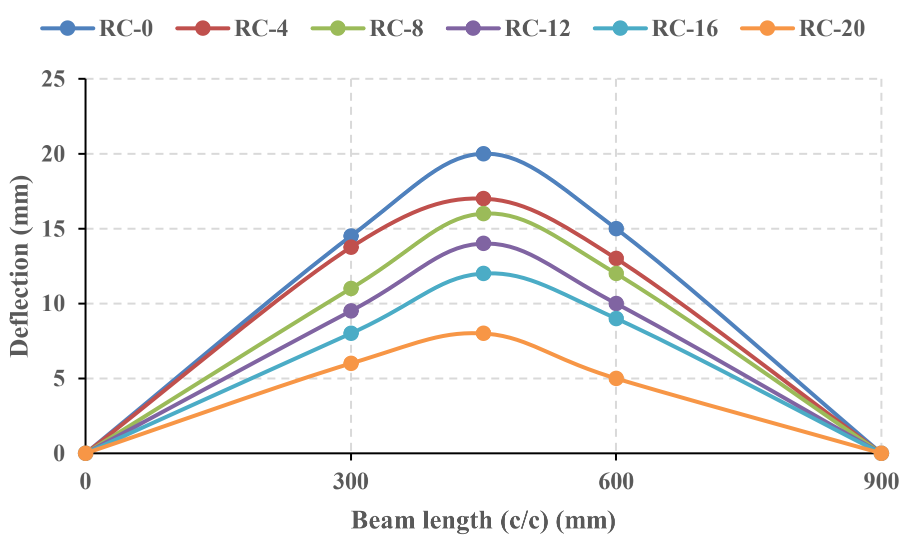

Fig. 23. Deflected profile

4.4 FEM Validation and Parametric Study

4.4.1 Validation

The developed nonlinear FEM was validated by comparing numerical predictions against experimental results for all six RC beams in terms of ultimate load and corresponding deflection (Table 14). The model consistently (Fig. 24) overestimates both quantities, with percentage errors ranging from approximately 5% to 14%, average errors of 9.11% for load and 9.15% for deflection, a level of discrepancy considered acceptable for CDP-based nonlinear modelling of RC structures, which inherently tends toward slight stiffness and strength overestimation. Marginally higher errors at RC-8 and RC-20 reflect the increased difficulty of capturing bond degradation, crack localisation, and brittle failure mechanisms under elevated contamination. Statistical validation confirms the model's accuracy: MAE = 3.02 kN and RMSE = 3.18 kN for load, and MAE = 1.40 mm and RMSE = 1.48 mm for deflection, with coefficients of determination of $R^2 = 0.995$ (load) and $R^2 = 0.993$ (deflection), indicating excellent correlation between numerical and experimental responses across all contamination levels. The low and consistent error values show that the ABAQUS model is appropriate for the following parametric study and is able to capture the stiffness degradation, peak load and post-cracking behaviour.

TABLE XIV. FEM VS. EXPERIMENTAL PROGRAMME

Beam	Exp. Pu (kN)	FE Pu (kN)	Exp. Δ (mm)	FE Δ (mm)	% Error (Pu)	% Error (Δ)	Exp./FE (Pu)	Exp./FE (Δ)
RC-0	47	50.54	20	21.28	7.53	6.40	0.93	0.94
RC-4	44.5	48.37	17	18.68	8.70	9.88	0.92	0.91
RC-8	38	42.70	16	17.98	12.37	12.38	0.89	0.89
RC-12	31.5	33.16	14	15.91	5.27	13.64	0.95	0.88
RC-16	25	27.47	12	13.04	9.88	8.67	0.91	0.92
RC-20	18.3	20.80	8	8.51	13.66	6.38	0.88	0.94
Mean							0.92	0.91
SD							0.03	0.02
CoV							2.80	2.51

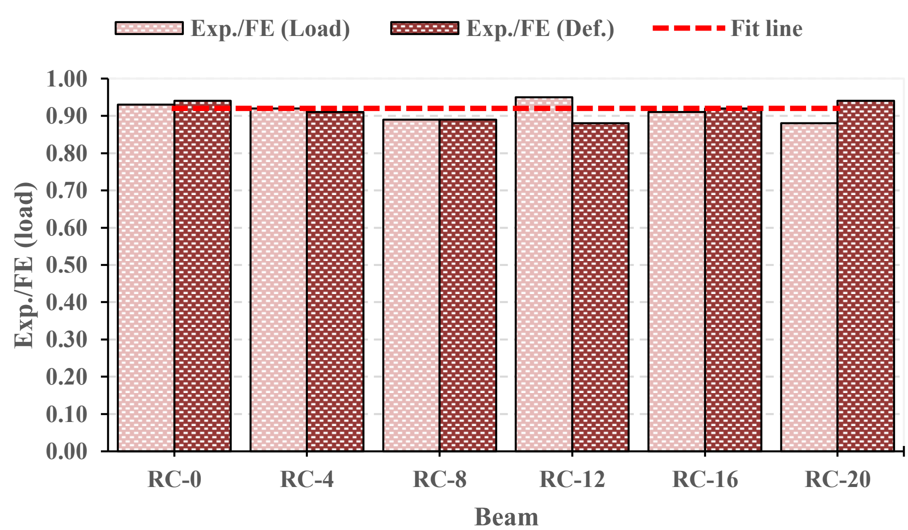

Fig. 24. Peak results accuracy Exp. vs FE

4.4.2 Failure Modes Predicted by the Finite Element Model

The PEEQ contours are in line with the classical ductile under-reinforced flexural failure seen in the control beam RC-0 (Fig. 25) that began at midspan on the bottom of the beam and moved up at regular increments of approximately 95–110 mm with the PEEQ contours reinforcing that compressive plastic strain was concentrated in the bottom extreme compression fibre (fibre) only near the expected ultimate load of 50.54 kN, in agreement with the experimental ultimate load of 47.0 kN and the observed plastic plateau between 15 and 25 mm of deflection. Since there is no tensile plastic strain along the trajectory of reinforcement, it means a perfect bond and steel yield control after the peak. The compressive plastic strain zone is similar in extent but is found to occur at a lower predicted load (48.37 kN) and there is no development of splitting strains along the placement of reinforcement, so the failure mode is still ductile flexural crushing, though with some slight deterioration in bond that is only apparent numerically. The most important qualitative change is at RC-8 and RC-12 (see Fig. 27). In RC-8 (predicted Pu = 42.70 kN), the PEEQT contours reveal a secondary horizontal band of tensile plastic strain developing along the longitudinal reinforcement within the shear span, absent in RC-0 and RC-4 (refer to Fig. 26), representing the onset of bond-splitting at the oil-contaminated bar–concrete interface. In RC-12, this horizontal splitting band is considerably more extensive and of higher magnitude, combining with localised midspan compression crushing to produce a mixed flexural–bond-splitting failure mode that explains the more abrupt experimental load–deflection response at this contamination level. At RC-16 and RC-20 (Fig. 28), bond-splitting governs failure entirely. In RC-16 (predicted Pu = 27.47 kN), a continuous horizontal PEEQT band extends along the reinforcement from midspan to within 150 mm of the supports, with minimal vertical crack development, confirming that loss of composite action, rather than compressive crushing, terminates the structural response. In RC-20 (predicted Pu = 20.80 kN), the splitting zone traverses virtually the full beam length between supports, with negligible compressive plastic strain at midspan, consistent with the experimentally observed explosive failure and the numerically predicted ultimate deflection of 8.51 mm, a 60% reduction relative to the 21.28 mm predicted for RC-0. Table 15 illustrates the failure mode comparisons.

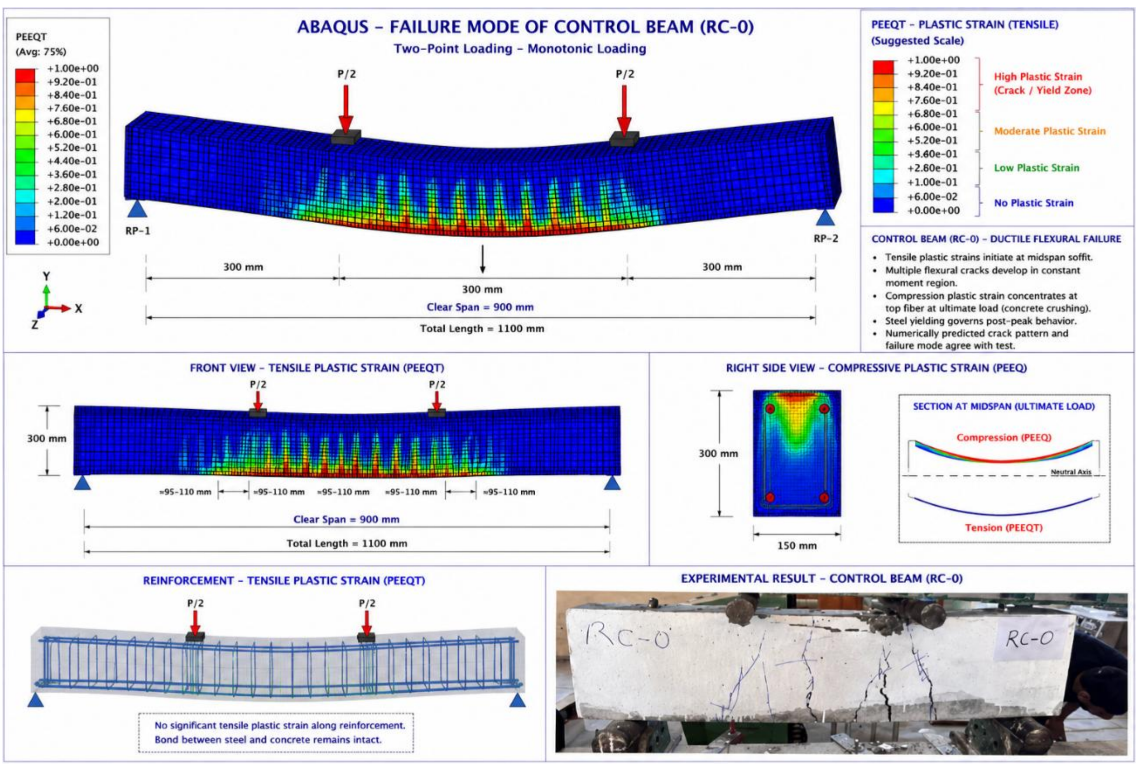

Fig. 25. Zero contamination

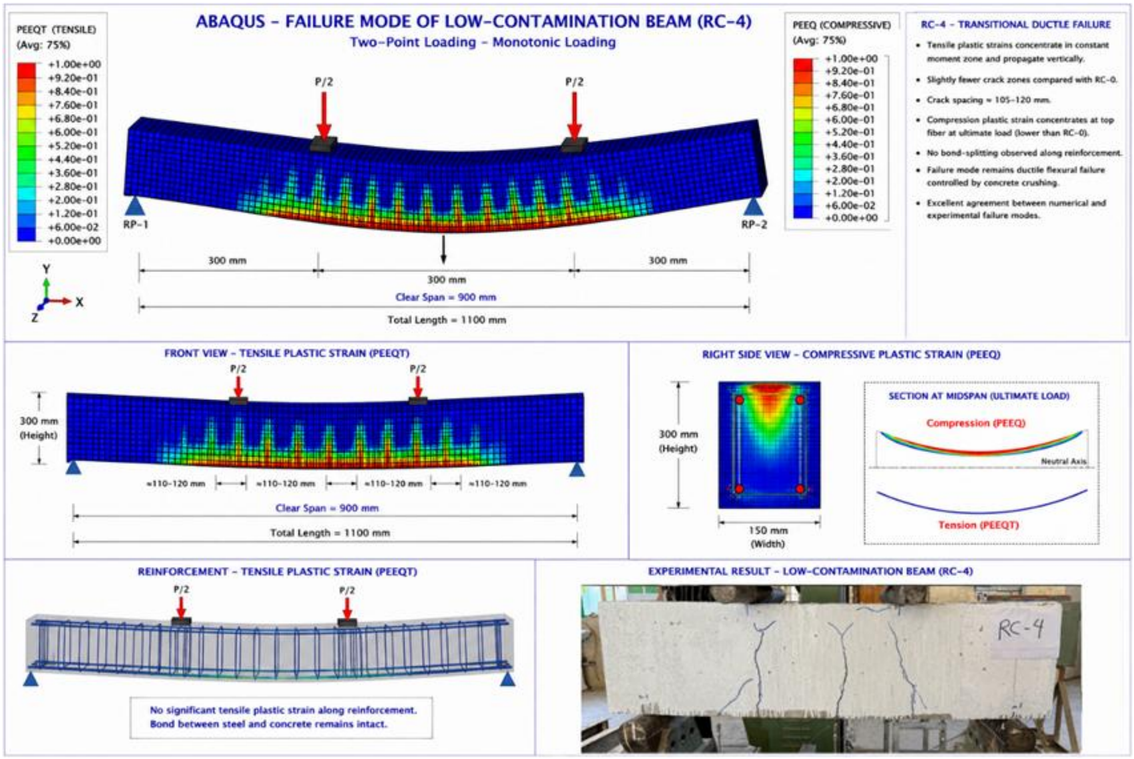

Fig. 26. Low contamination

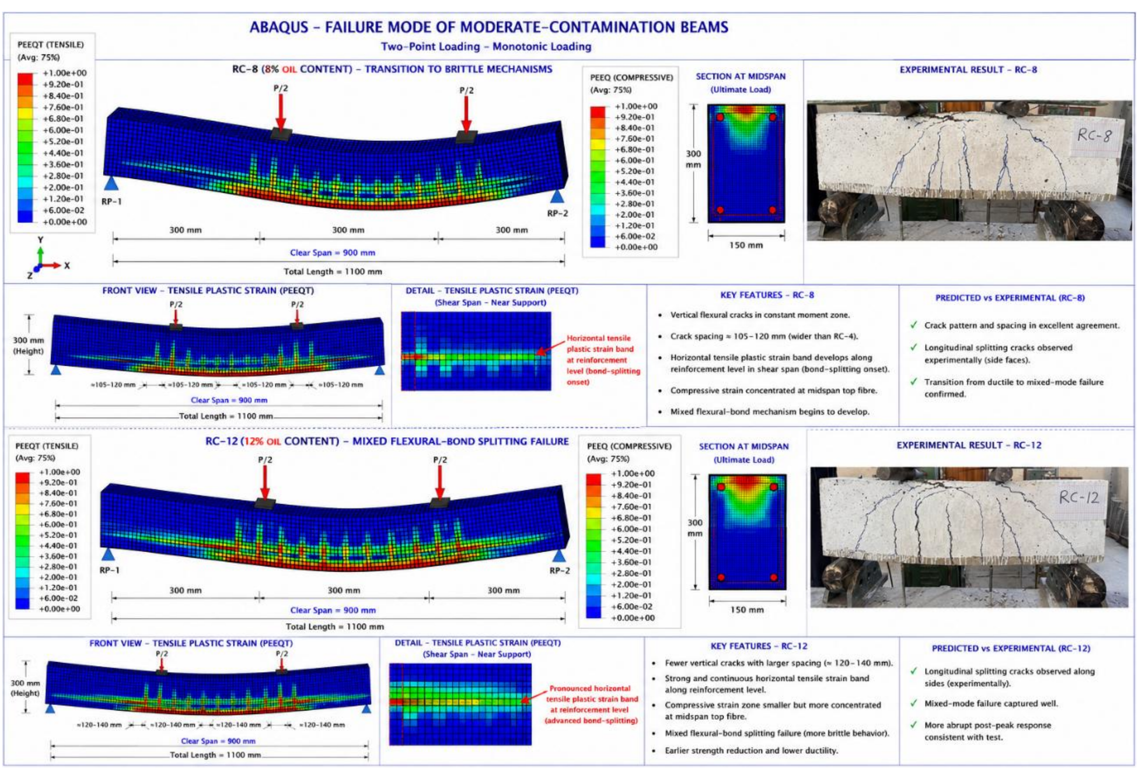

Fig. 27. Moderate contamination

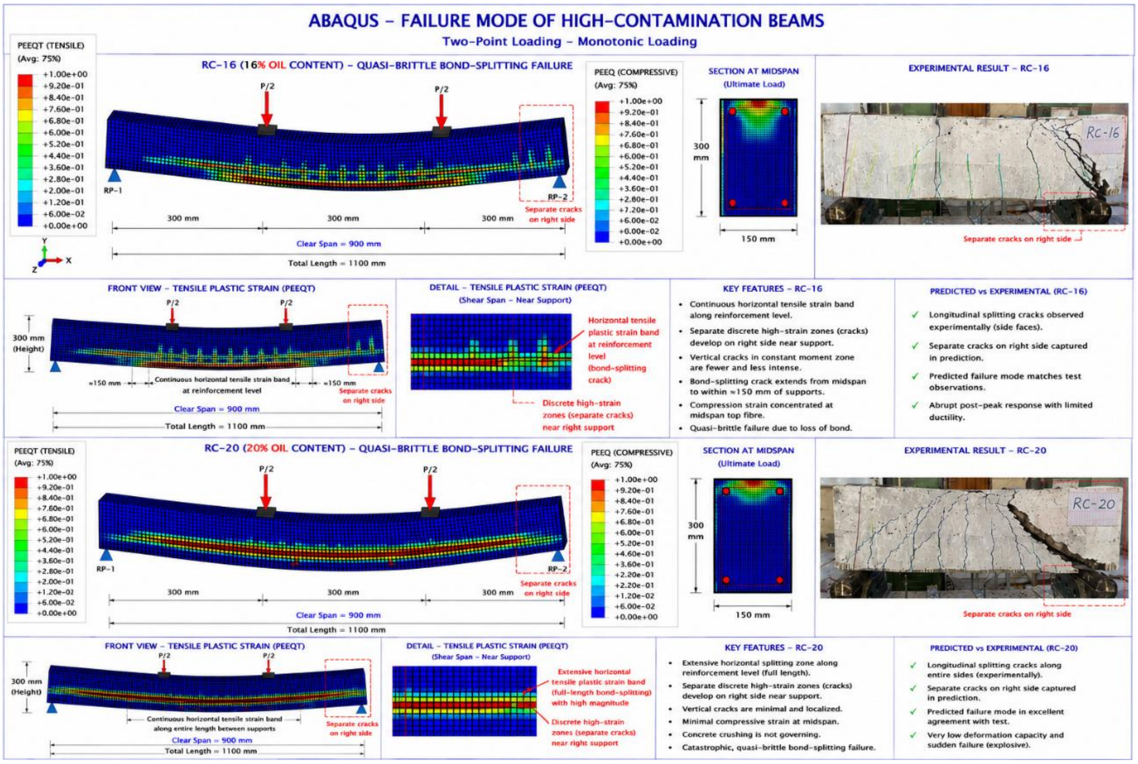

Fig. 28. High contamination

TABLE XV. COMPARISON OF NUMERICALLY PREDICTED AND EXPERIMENTALLY OBSERVED FAILURE MODES

Beam	Predicted Failure Mode (FEM)	Exp. Failure Mode	Agreement
RC-0	Compression crushing at midspan (ductile)	Ductile flexural compression	Excellent
RC-4	Compression crushing - slightly narrower crack band	Ductile flexural compression	Excellent
RC-8	Mixed: flexural + onset of bond-splitting	Mixed - early splitting cracks	Very Good
RC-12	Mixed: flexural + moderate bond-splitting	Mixed flexural-splitting	Very Good
RC-16	Bond-splitting dominant + limited crushing	Quasi-brittle splitting	Good
RC-20	Full bond-splitting - catastrophic	Explosive/brittle failure	Good

4.4.3 Parametric Study

Following successful model validation, a systematic parametric investigation was conducted using the calibrated ABAQUS model to characterise the sensitivity of structural performance to five design variables, compressive strength, stirrup spacing, beam clear span, boundary conditions, and extended contamination level, each varied independently relative to a reference configuration of 38.43 MPa, 100 mm stirrup spacing, 900 mm clear span, simply supported conditions, and 20% oil contamination (Figs. 29–33). The increase in compressive strength from 30 MPa to 50 MPa (Fig. 29) has a corresponding increase in ultimate load of approximately 13.8% and a decrease at the lower grade of approximately 10.6% without any significant change in the proportion of the increase or decrease in ultimate load throughout the various contamination levels because flexural strength is only as strong as the tensile strength of the reinforcement at the under-reinforced section behaviour. The absolute benefit from upgrading, however, is significant reduction with contamination; the improvement in compressive strength from an upgrade is around 7.0 kN per 50 MPa for 0% contamination and 2.9 kN per 50 MPa for 20% contamination showing that compressive strength gains are not adequate to compensate for losses in bond capacity caused by ITZ degradation due to contamination. Interestingly, the load values of all the 50 MPa grades at 20% contamination are lower than the 30 MPa one at 0% contamination, highlighting contamination level as the most important performance variable.

The effects of varying the stirrup spacing, from 100 mm to 200 mm, on the ultimate load value is presented in Fig. 30. It is seen that the ultimate load increases by about 7.5% when the spacing of the stirrups decreases from 100 mm to 75 mm; however, it drops by about 19.1% when the spacing is increased from 100 mm to 200 mm for the whole range of contamination. Both these variations with stirrup spacing are consistent across the entire range of contamination. However, there is a reduction in the absolute benefit of closer spacing as contamination increases, from 3.8 kN at 0 % to 1.5 kN at 20 % due to progressive bond degradation reducing the effectiveness of lateral confinement to resist splitting forces. The ultimate load for this combination of 200 mm spacing and 20% contamination is predicted to be 16.8 kN, with a midspan deflection of only 7.0 mm, a reduction of about 66.7% compared to the uncontaminated reference beam, and showing that the combination of wide spacing and high contamination levels is structurally unsafe, with low strength and very little ductility.

Fig. 31 indicates that the 750 mm span (a/d ≈ 1.56) has about 17 percent higher ultimate loads than the reference for the range of contaminations considered, while the 1200 mm span (a/d ≈ 2.50) has about 18 percent lower loads and midspan deflections at failure about 37 percent higher than the reference. The shorter span comprises some structural redundancy because of the compressive arch action, which requires less tensile bond than does the conventional beam bending, and provides some tolerance for the bond-splitting effects at high contamination levels where PEEQT contours indicate a less extensive horizontal splitting crack pattern on the 750 mm models. The 1200 mm span, on the other hand, is highly dependent on the continuous bond and requires a long length of reinforcement, and shows a more extensive bond-splitting zone, the load at 20% contamination is only 41% of its clean-concrete capacity, indicating that long-span beams in contaminated concrete structures should be subject to greater scrutiny during structural assessment.

Fig. 32 shows that the ultimate load in the case where the beam is simply supported on both ends and is then fixed-pinned at both ends, is about 10.6% higher, consistently across all levels of contamination; and the fully fixed-fixed condition is about 24.5% higher, consistently across the same contamination levels. End restraint (ER) influences the structural performance by two mechanisms: Firstly, the bending moment redistribution mechanism decreases the load demand from the positive bending moments on the midspan section of the structure which is weakened by the oil contamination; Secondly, the compressive arching action provides a bond independent load path that becomes relatively more important as the tensile bond mechanism weakens due to the oil contamination. The absolute load advantage of end restraint is reduced from 12.4 kN at 0% to 5.1 kN at 20% for the fixed-fixed configuration, and the midspan deflection under fixed-fixed conditions is reduced to 5.5 mm at 20% contamination, indicating that whilst end restraint offers a consistent proportional improvement in load capacity it cannot restore the ductility lost on incurring severe bond-splitting failure.

Extrapolating outside the range of validation (see Fig. 33) shows a steady worsening but slowing degradation that seems to correspond to the physical saturation of the aggregate above about 20% oil content. At 32% contamination, the beam has less than 10% of its load-carrying capacity when it fails, and its deflections at failure are less than 10% of its span, which is imperceptible during normal structural service life, implying that no warning signs are discernable before failure. This capacity and deformation warning progressive elimination gives the necessary quantitative justification for limiting the amount of aggregate impurities to less than about 10 – 15% in all structures of safety critical importance.

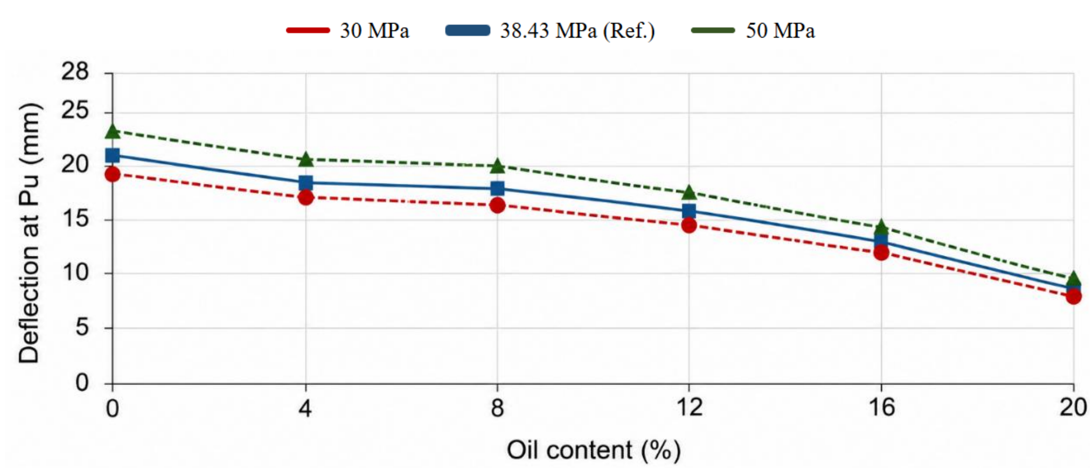

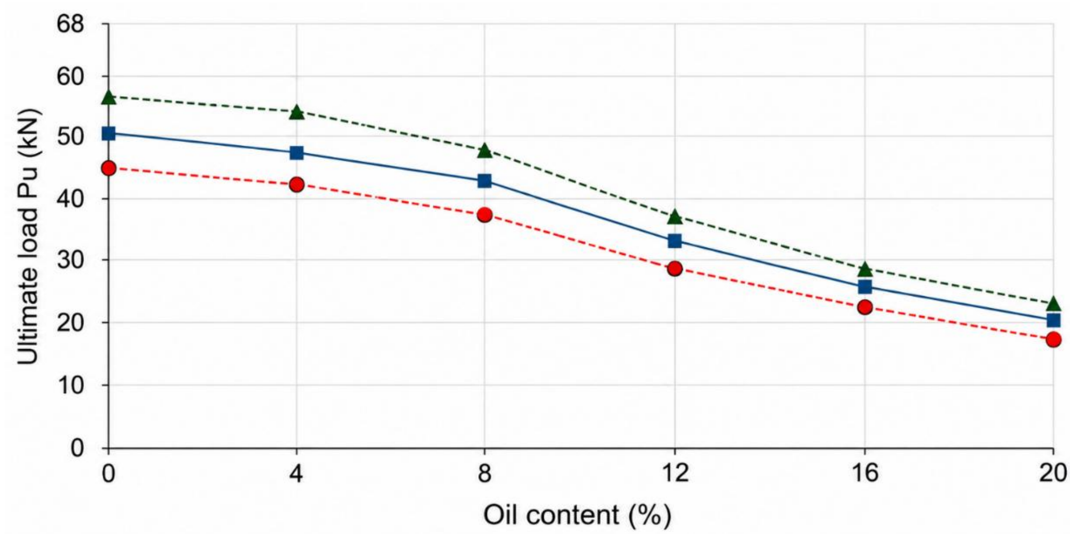

Fig. 29. Impact of *fc'*: Load and deflection vs. oil content

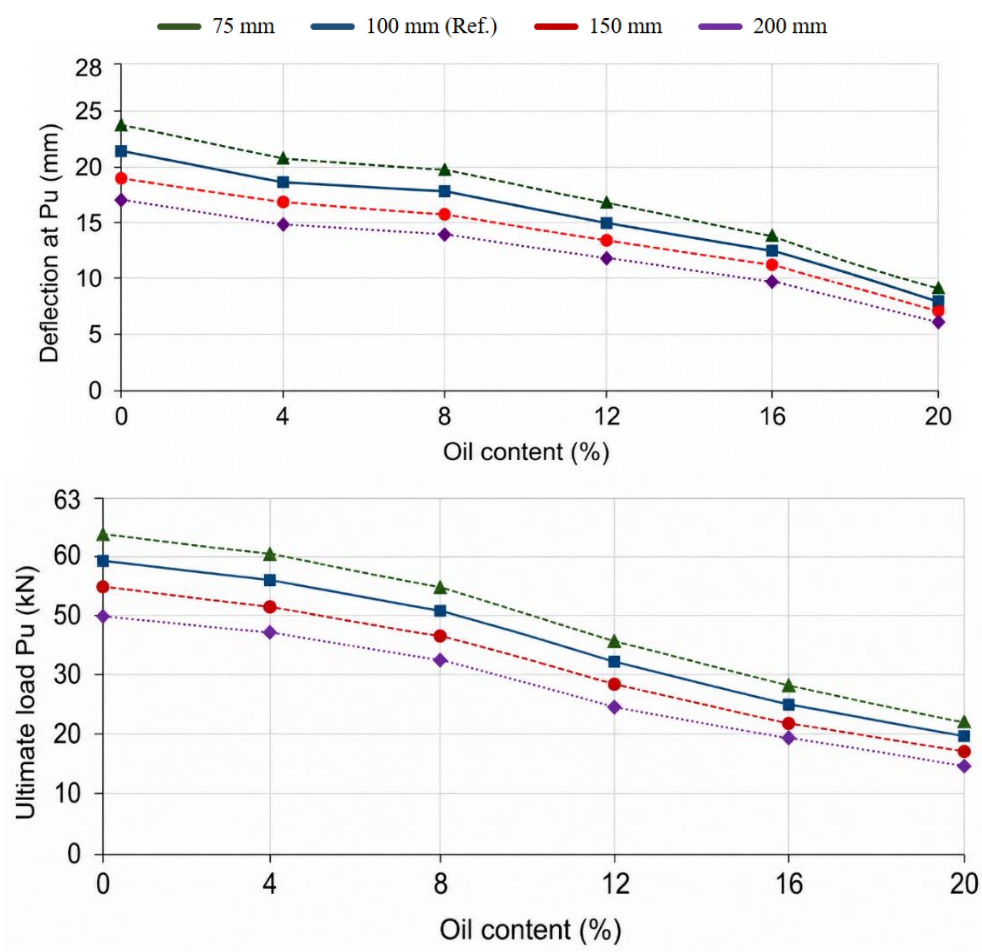

Fig. 30. Impact of bar spacing: Load and deflection vs. oil content

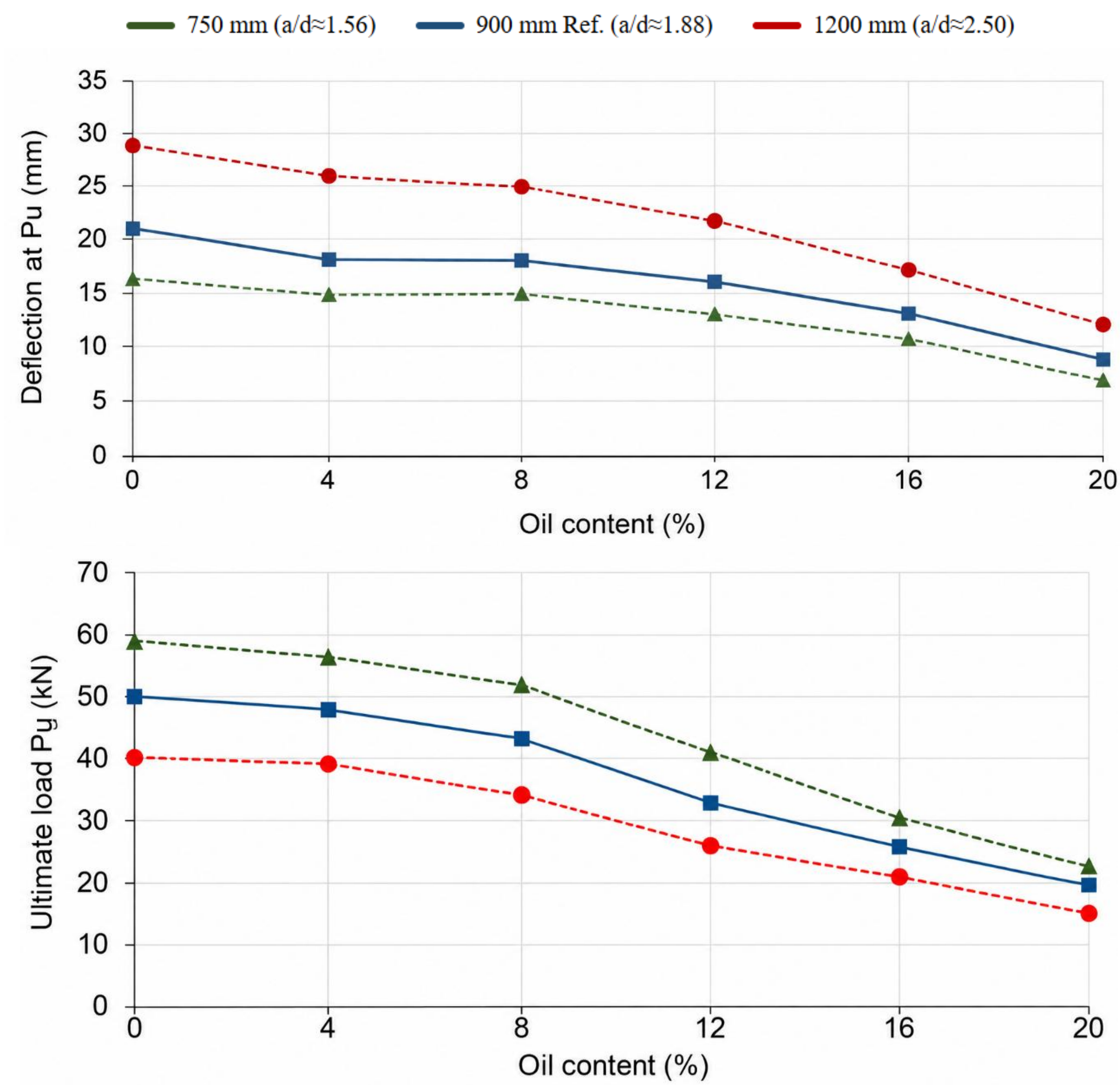

Fig. 31. Impact of clear span: Load and deflection vs. oil content

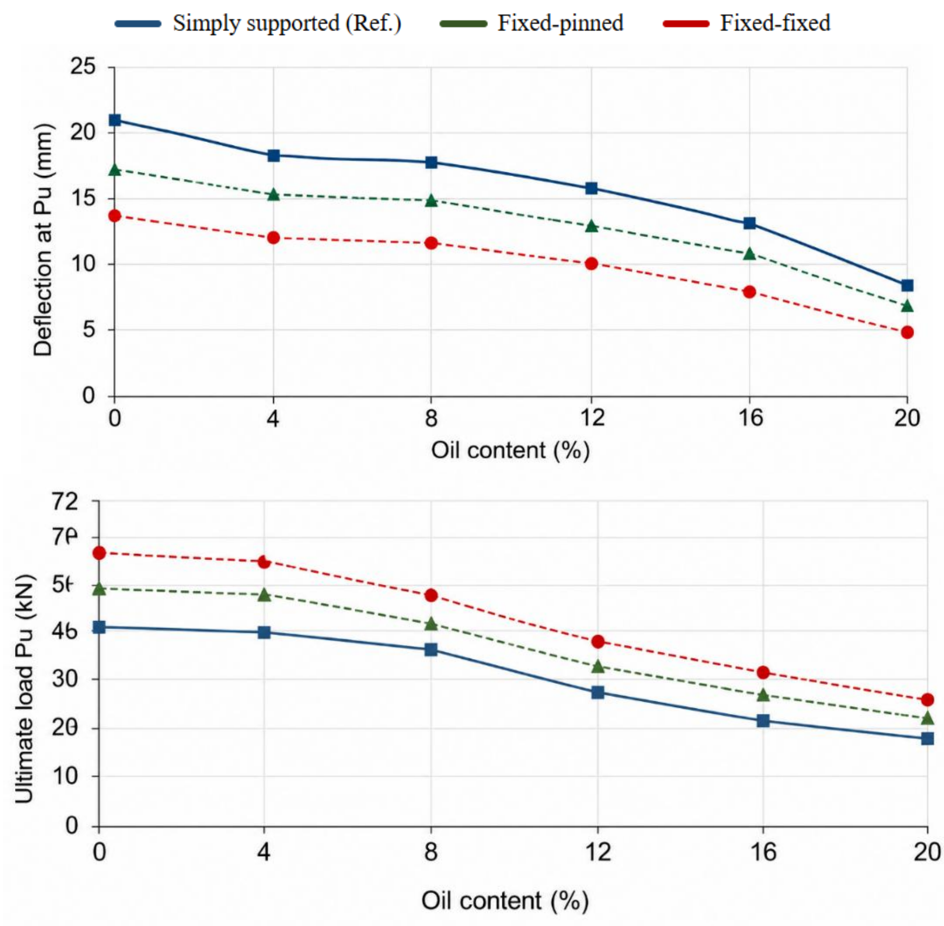

Fig. 32. Impact of boundary condition: Load and deflection vs. oil content

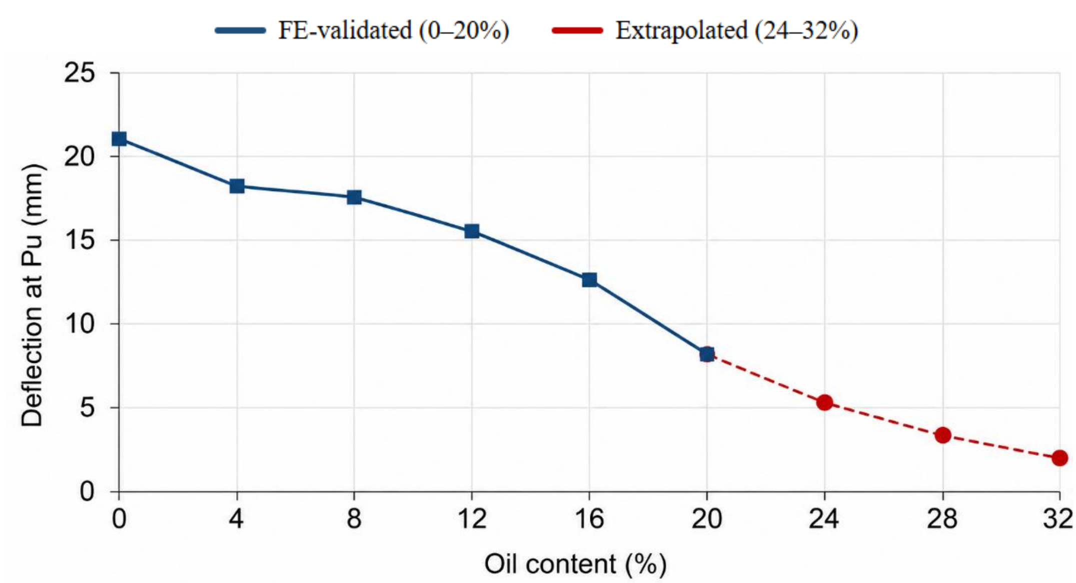

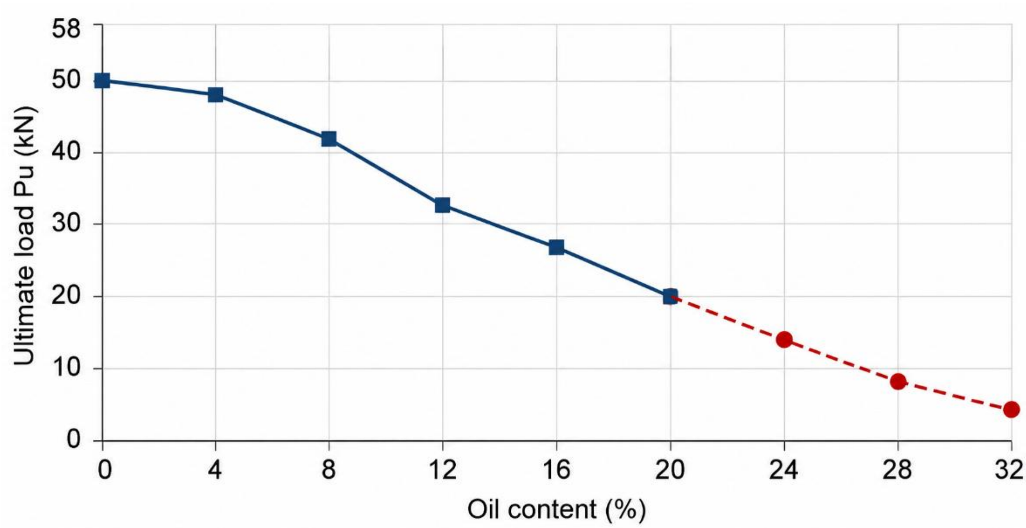

Fig. 33. Impact of extended contamination: Load and deflection vs. oil content

5. ENGINEERING IMPLICATIONS AND LIMITATIONS

The results enable a practical limit value of 8–12% for contamination level to be applied for structural RC applications; if the contamination level is less than 8%, the structural performance of the material is reduced, but this can be mitigated with conservative design changes; contamination levels exceeding 12% cause the material to become brittle and unable to resist ductile behaviour, which is required in modern seismic design codes. The threshold should be used as a guide for acceptance criteria for aggregates in specifications used for oil producing areas. While this is of scientific interest, the small magnitude of the marginal improvement at 2% oil content and its sensitivity to increasing contamination, does not provide a scientific basis for intentional addition of oil to concrete mixtures: the benefit is only realised within a very narrow range of contamination, and is rapidly lost with increasing contamination. The parametric study results indicate that, when low level contamination (0.04%) cannot be avoided, moderate gains in compressive strength and reduced spacing of stirrups and appropriate span selection can help to offset this. But it is not enough with these measures if contamination is more than 8%.

The constraints of this study are: (1) contaminants were introduced under controlled laboratory conditions and tested with a single source of crude oil, whereas hydrocarbons would be found in contamination in the field with different compositions, ageing effects, and non-uniform distribution, (2) the FEM model assumes perfect bond, which may not be true at high levels of contamination; (3) the study was carried out under monotonic loading conditions, with behaviour in cyclic, impact and sustained loading conditions yet to be characterised; and (4) long-term durability, such as chloride ingress, carbonation and creep effects, was not considered.

6. CONCLUSION AND FUTURE RESEARCH

From the experimental and numerical study of a reinforced concrete made with crude oil-contaminated sand, the following conclusions were drawn:

1. The percentage of water absorption rises by about 249%, the specific gravity drops by 7.3% and bulk density rises by 8.6% compared to clean sand due to crude oil contamination. Continued oil coating on the grain surface was confirmed by SEM, small lattice distortion and decreased crystallite size was established by XRD, and increased hydrocarbon-derived carbon content was confirmed by EDS. The levels of heavy metals were not detected as hazardous.
2. The marginal improvement in all mechanical properties of concrete with 2% oil content is followed by progressive nonlinear deterioration. Compressive strength, splitting tensile strength, modulus of rupture, and modulus of elasticity are decreased by 70.91%, 89.94%, 71.43%, and 44.84%, respectively at 30% oil content. Splitting tensile strength is most sensitive property, which is highly interdependent with the quality of the transition zone between interfaces.
3. The performance of the RC beam structure decreases systematically as the oil contamination increases, The results show that cracking load decreases by 70.0% and ultimate load decreases by 61.1% from 0% to 20% oil

content while midspan deflection decreases by 60.0% from 0% to 20% oil content. It can be seen from the cracking load reduction that they are generally higher than the ultimate load reduction, which is a confirmation of the tensile-governed behaviour being more vulnerable than bulk compressive behaviour.

4. The change in failure mode and the transition from ductile flexural failure with a more uniform distribution of cracking and post-peak deformation to brittle and explosive failure with much more localised cracking, loss of energy absorption and no real warning before collapse occurs is very fundamental and structurally critical, at 8-12% oil content. The transition is controlled by the degradation of steel–concrete bond and integrity of ITZ caused by the oil-coating of aggregate particles.
5. The 5th criterion is that beyond 8–12% contamination, OCS concrete is structurally unsuitable for applications with requirements for ductility, seismic resistance and/or occupant safety.
6. The validated nonlinear FEM (R^2 = 0.995 for load, 0.993 for deflection) accurately represents experimental behaviour for all contamination levels and the parametric study shows that no combination of structural parameters removes the penalty of oil contamination greater than 20%.

Based on the limitations and findings of this study, the following research directions are recommended:

1. As dramatically demonstrated herein, energy absorbability reduced under monotonic loading, cyclic and seismic loading tests are necessary to quantify the energy dissipation capacity and cumulative damage behaviour of OCS-RC members.
2. The mechanical and structural properties of OCS concrete should be recovered partially by fibre reinforcement (steel, polypropylene and basalt) and supplementary cementitious materials (fly ash, silica fume and GGBS) and should be studied systematically.
3. Under sustained loading and multiple exposures to carbonation, chloride ingress and wet–dry cycling, long-term durability needs to be evaluated, given that the high-water absorption of OCS is of concern for moisture-assisted degradation during service life.
4. Extension of the experimental programme to RC slabs, columns, and CFST members incorporating OCS would characterise the influence of confinement and biaxial stress states on contamination-induced degradation.
5. Machine learning-based predictive models trained on the present dataset could provide generalised assessment tools for contaminated concrete in practice.
6. Life-cycle assessment (LCA) comparing OCS reuse against conventional disposal would support evidence-based sustainability policy in petroleum-affected regions.

Conflict of Interest

No conflict of interest is registered

Funding

This research received no external funding.

Available Data

The data is available upon reasonable requesting

Acknowledgment

None.

References

[1] A. K. Ahmed and R. A. Mahmood, "The effect of oil contamination on some geotechnical properties of West Qurna oilfield soils at Basrah, Southern Iraq," *Iraqi Geol. J.*, pp. 76–84, 2021, doi: 10.46717/igj.54.2B.7Ms-2021-08-27.

[2] S. N. Abdulhamid, A. M. Hasan, and S. Q. Aziz, "Solidification/stabilization of contaminated soil in a south station of the Khurmala oil field in Kurdistan region, Iraq," *Appl. Sci.*, vol. 11, no. 16, Art. no. 7474, 2021, doi: 10.3390/app11167474.

[3] O. A. Wasiu, "Effect of crude oil contaminated sand on the engineering properties of concrete," University of Ibadan, 2013. [Online]. Available: http://hdl.handle.net/123456789/148

[4] M. M. Kadhum, N. A. Alwash, W. K. Tuama, and M. S. Abdulraheem, "Experimental and numerical study of influence of crude oil products on the behavior of reactive powder and normal strength concrete slabs," *J. King Saud Univ. Eng. Sci.*, vol. 32, no. 5, pp. 293–302, 2020, doi: 10.1016/j.jksues.2019.03.007.

[5] R. Abousnina and R. L. Allister, *Oil Contaminated Sand: Sources, Properties, Remediation, and Engineering Applications*. London, U.K.: IntechOpen, 2022, doi: 10.5772/intechopen.103802.

[6] A. Al-Rawas, H. F. Hassan, R. Taha, A. Hago, B. Al-Shandoudi, and Y. Al-Suleimani, "Stabilization of oil-contaminated soils using cement and cement by-pass dust," *Manag. Environ. Qual. Int. J.*, vol. 16, no. 6, pp. 670–680, 2005, doi: 10.1108/14777830510623736.
[7] J. Domski, "Long-term study on fibre reinforced fine aggregate concrete beams based on waste sand," *Rocz. Ochr. Środowiska*, vol. 17, no. 1, pp. 188–199, 2015.
[8] R. M. Abousnina, A. Manalo, and W. Lokuge, "Physical and mechanical properties of cement mortar containing fine sand contaminated with light crude oil," *Procedia Eng.*, vol. 145, pp. 250–258, 2016, doi: 10.1016/j.proeng.2016.04.071.
[9] R. Abousnina, A. Manalo, W. Ferdous, W. Lokuge, B. Benabed, and K. Saif Al-Jabri, "Characteristics, strength development and microstructure of cement mortar containing oil-contaminated sand," *Constr. Build. Mater.*, vol. 252, Art. no. 119155, 2020, doi: 10.1016/j.conbuildmat.2020.119155.
[10] H. A. Al-Sanad, W. K. Eid, and N. F. Ismael, "Geotechnical properties of oil-contaminated Kuwaiti sand," *J. Geotech. Eng.*, vol. 121, no. 5, pp. 407–412, May 1995, doi: 10.1061/(ASCE)0733-9410(1995)121:5(407).
[11] R. Abousnina, A. Manalo, W. Lokuge, and K. S. Al-Jabri, "Properties and structural behavior of concrete containing fine sand contaminated with light crude oil," *Constr. Build. Mater.*, vol. 189, pp. 1214–1231, 2018, doi: 10.1016/j.conbuildmat.2018.09.089.
[12] M. Khamehchiyan, A. H. Charkhabi, and M. Tajik, "Effects of crude oil contamination on geotechnical properties of clayey and sandy soils," *Eng. Geol.*, vol. 89, nos. 3–4, pp. 220–229, 2007, doi: 10.1016/j.enggeo.2006.10.009.
[13] E. Khosravi, H. Ghasemzadeh, M. R. Sabour, and H. Yazdani, "Geotechnical properties of gas oil-contaminated kaolinite," *Eng. Geol.*, vol. 166, pp. 11–16, 2013, doi: 10.1016/j.enggeo.2013.08.004.
[14] G. C. Ezeokpube, G. U. Alaneme, I. C. Attah, I. M. Udousoro, and D. Nwogbo, "Experimental investigation of crude oil contaminated soil for sustainable concrete production," *Archit. Struct. Constr.*, vol. 2, no. 3, pp. 349–364, 2022, doi: 10.1007/s44150-022-00069-2.
[15] S. O. Osuji and E. Nwankwo, "Effect of crude oil contamination on the compressive strength of concrete," *Niger. J. Technol.*, vol. 34, no. 2, pp. 259–265, 2015, doi: 10.4314/njt.v34i2.7.
[16] M. Attom, R. Hawileh, and M. Naser, "Investigation on concrete compressive strength mixed with sand contaminated by crude oil products," *Constr. Build. Mater.*, vol. 47, pp. 99–103, 2013, doi: 10.1016/j.conbuildmat.2013.04.042.
[17] H. Diab, "Compressive strength performance of low- and high-strength concrete soaked in mineral oil," *Constr. Build. Mater.*, vol. 33, pp. 25–31, 2012, doi: 10.1016/j.conbuildmat.2012.01.015.
[18] H. Diab, "Effect of mineral oil on reinforced concrete structures. Part I: Deterioration of compressive strength," *JES. J. Eng. Sci.*, vol. 39, no. 6, pp. 1321–1333, 2011, doi: 10.21608/jesaun.2011.129426.